

Scrutinizing Vacuum Stability in IDM with Type-III Inverse seesaw

Priyotosh Bandyopadhyay,^a Shilpa Jangid,^a Manimala Mitra^{b,c}

^a*Indian Institute of Technology Hyderabad, Kandi, Sangareddy-502287, Telangana, India*

^b*Institute of Physics, Sachivalaya Marg, Bhubaneswar 751005, India*

^c*Homi Bhabha National Institute, BARC Training School Complex, Anushakti Nagar, Mumbai 400094, India*

E-mail: bpriyo@phy.iith.ac.in, ph19resch02006@iith.ac.in,
manimala@iopb.res.in

ABSTRACT: We analyze the vacuum stability for the inert Higgs doublet extension of the Standard Model (SM), that also contains two sets of $SU(2)_L$ triplet fermions with hypercharge zero. The model represents a Type-III inverse seesaw mechanism for neutrino mass generation with a Dark matter candidate. An effective potential approach calculation with two-loop beta function have been carried out in deciding the fate of the electroweak vacuum. Weak gauge coupling g_2 shows a different behaviour as compared to the Standard Model. The modified running of g_2 , along with the Higgs quartic coupling and Type-III Yukawa couplings become crucial in determining the stability of electroweak vacuum. The interplay between two and three generations of such triplet fermions reveals that extensions with two generations is favoured if we aspire for Planck scale stability. Bounds on the Higgs quartic couplings, Type-III Yukawa and number of triplet fermion generations are drawn for different mass scale of Type-III fermions. The phenomenologies of inert doublet and Type-III fermions at the LHC and other experiments are commented upon.

KEYWORDS: Beyond Standard Model, Extended Higgs Sector, Vacuum Stability, Type-III Seesaw, Inverse Seesaw

Contents

1	Introduction	1
2	The Model	3
2.1	The Scalar Sector	3
2.2	The Type-III and Inverse Seesaw Lagrangians	4
3	Perturbativity	7
3.1	Running of Gauge couplings:	7
4	Stability Bound	14
4.1	RG Evolution of the Scalar Quartic Couplings	15
4.2	Variation perturbativity and stability with Y_N	17
4.3	Vacuum Stability from RG-improved potential Approach	20
4.4	Effective Potential	20
4.5	Stable, Metastable and Unstable Regions	22
5	Discussions and conclusion	26
A	Two-loop β-functions-With two generations	27
A.1	Scalar Quartic Couplings	27
A.2	Yukawa Coupling	30

1 Introduction

Higgs boson was the last missing piece of the Standard Model (SM) which was discovered at the CMS and ATLAS detectors of the Large Hadron Collider (LHC) [1, 2]. The spin, parity measurements and the combined analysis show the SM-like behaviour of the Higgs boson [3–5]. However it has been shown that Standard Model electroweak (EW) vacuum on its own can run into metastability due to quantum corrections [6–9]. It is well known that the addition of scalars enhance the stability of the EW vacuum via positive loop contributions to the Higgs quartic coupling. Various models, which include scalars from different gauge representations have been proposed [10–18] to enhance the stability of EW vacuum. On the contrary an extension with fermion often gives negative contributions to the Higgs quartic couplings that it couples to. Such negative contributions then tend to pull such Higgs quartic couplings toward instability much faster. Thus models with extra fermions, where

Majorana masses of the fermions are spontaneously generated are constrained from the vacuum stability [19, 19–40].

Apart from the problem of vacuum metastability in SM which depends on the top quark and Higgs boson masses [41–43], the theory also fails to provide a stable dark matter (DM) candidate, as well as to give successful explanation for the very tiny eV scale neutrino masses, and their mixings. In this work, we focus on these two aspects by extending the SM with $SU(2)_L$ triplet fermions, and $SU(2)_L$ inert doublet scalar. The triplet fermion generates the eV light neutrino mass via Type-III seesaw mechanism, while the inert Higgs doublet provides a dark matter candidate, as well as stabilizes the EW vacuum.

The minimal Type-III extensions have one to three generations of $SU(2)_L$ fermions with hypercharge zero, which mix with the SM charged and neutral fermions, and also generates tiny eV neutrino mass via electroweak symmetry breaking[44–46]. Different extensions of Type-III seesaw and their collider signatures have been studied in [47]–[53], including their spin measurement at the LHC [54]. The stability of EW vacuum in some these scenarios are studied in [55–58]. In this article, we consider the inverse seesaw mechanism of neutrino mass generation with two generations triplet fermions. One among them couples with the SM Higgs boson via Type-III Yukawa coupling, and generates the Dirac mass term. The other triplet fermion generates the Majorana mass term for the triplet fermion.

As discussed earlier an extension with scalar enhances stability of EW vacuum and if the scalar is in the form of $SU(2)_L$ inert (Z_2 -odd) doublet then it also provides the much needed dark matter candidate [14]. SM extension with such inert doublet in the context of vacuum stability have been studied extensively[14–16, 19]. Fields in inert doublet have very interesting phenomenology due to their compressed spectrum and the possibility of real and pseudoscalar dark matter particle [59]–[70]. In this article we will investigate the effect of inert doublet in the context of Type-III fermions.

In our model we have both $SU(2)_L$ triplet fermion and $SU(2)_L$ doublet scalar. Being in the triplet representation of $SU(2)_L$ the new fermions contribute in the evolution of weak gauge coupling g_2 such that g_2 now increases with running scale. This behaviour substantially changes the dynamics of couplings responsible for the EW vacuum stability. We shall see how an enhanced g_2 causes a much lower perturbative scale compared to Type-I [19] or only IDM case [16]. Specially we see that with three generations of Type-III fermions it is difficult to attained Planck scale perturbativity and thus two generations are more favoured.

The paper is organised as follows. In section 2, we describe the model, and present the EW symmetry breaking conditions for this model. We discuss the perturbativity and the interplay of two and three generations of $SU(2)_L$ triplet fermions in section 3. The EW vacuum stability with all three possibilities are covered in section 4. In section 5, we discuss the phenomenological consequences and present our

conclusion. For completeness, we give the expressions for two-loop beta functions used in our analysis in [Appendix A](#).

2 The Model

We extend the SM with an inert doublet (ID) and three Type-III fermions with ISS mechanism. The scalar sector of the model is discussed in [Section 2.1](#). For the vacuum stability analysis, we consider two different scenarios, viz., a canonical type-III seesaw with small Yukawa couplings and an inverse seesaw with large Yukawa couplings. The fermionic sector with Type-III seesaw and inverse seesaw is discussed in [Section 2.2](#).

2.1 The Scalar Sector

The scalar sector of this model consists of two $SU(2)_L$ -doublet scalars Φ_1 and Φ_2 , both with the same hypercharge $1/2$:

$$\Phi_1 = \begin{pmatrix} G^+ \\ h + iG^0 \end{pmatrix}, \quad \Phi_2 = \begin{pmatrix} H^+ \\ H + iA \end{pmatrix}. \quad (2.1)$$

The tree-level scalar potential which is invariant under the SM gauge group $SU(2)_L \times U(1)_Y$ is given by [\[71, 72\]](#)

$$\begin{aligned} V_{\text{scalar}} = & m_{11}^2 \Phi_1^\dagger \Phi_1 + m_{22}^2 \Phi_2^\dagger \Phi_2 - (m_{12}^2 \Phi_1^\dagger \Phi_2 + \text{H.c}) \\ & + \lambda_1 (\Phi_1^\dagger \Phi_1)^2 + \lambda_2 (\Phi_2^\dagger \Phi_2)^2 + \lambda_3 (\Phi_1^\dagger \Phi_1) (\Phi_2^\dagger \Phi_2) + \lambda_4 (\Phi_1^\dagger \Phi_2) (\Phi_2^\dagger \Phi_1) \\ & + [\lambda_5 (\Phi_1^\dagger \Phi_2)^2 + \lambda_6 (\Phi_1^\dagger \Phi_1) (\Phi_1^\dagger \Phi_2) + \lambda_7 (\Phi_2^\dagger \Phi_2) (\Phi_1^\dagger \Phi_2) + \text{H.c}], \end{aligned} \quad (2.2)$$

where the mass terms m_{11}^2, m_{22}^2 and the Higgs quartic couplings $\lambda_{1,2,3,4}$ are all real. Whereas, m_{12}^2 and the $\lambda_{5,6,7}$ couplings are in general complex. To avoid the flavor changing neutral currents at tree-level and to make Φ_2 scalar as inert for getting a DM candidate, we impose an additional Z_2 symmetry under which Φ_2 is odd and Φ_1 is even. This removes the λ_6, λ_7 and m_{12} , terms from the potential and [Eq. \(2.2\)](#) reduces to

$$\begin{aligned} V_{\text{scalar}} = & m_{11}^2 \Phi_1^\dagger \Phi_1 + m_{22}^2 \Phi_2^\dagger \Phi_2 + \lambda_1 (\Phi_1^\dagger \Phi_1)^2 + \lambda_2 (\Phi_2^\dagger \Phi_2)^2 \\ & + \lambda_3 (\Phi_1^\dagger \Phi_1) (\Phi_2^\dagger \Phi_2) + \lambda_4 (\Phi_1^\dagger \Phi_2) (\Phi_2^\dagger \Phi_1) + [\lambda_5 (\Phi_1^\dagger \Phi_2)^2 + \text{H.c}]. \end{aligned} \quad (2.3)$$

The EW symmetry breaking is achieved by providing a real vacuum expectation value (VEV) to the first Higgs doublet, i.e

$$\langle \Phi_1 \rangle = \frac{1}{\sqrt{2}} \begin{pmatrix} 0 \\ v \end{pmatrix}, \quad (2.4)$$

with $v \simeq 246$ GeV. The second Higgs doublet Φ_2 , being Z_2 -odd, does not participate in the EW symmetry breaking (hence the name ‘inert 2HDM’). Using the minimization conditions, we express the mass parameter m_{11} in terms of other parameters as follows:

$$m_{11}^2 = -\lambda_1 v^2, \quad (2.5)$$

whereas the physical scalar masses are given by

$$\begin{aligned} M_h^2 &= 2\lambda_1 v^2, \\ M_{H_0}^2 &= \frac{1}{2}[2m_{22}^2 + v^2(\lambda_3 + \lambda_4 + 2\lambda_5)], \\ M_A^2 &= \frac{1}{2}[2m_{22}^2 + v^2(\lambda_3 + \lambda_4 - 2\lambda_5)], \\ M_{H^\pm}^2 &= m_{22}^2 + \frac{1}{2}v^2\lambda_3. \end{aligned} \quad (2.6)$$

This is to note that, since Φ_2 is inert, there is no mixing between Φ_2 and Φ_1 and the gauge eigenstates are same as the mass eigenstates for the Higgs bosons. The Z_2 -symmetry prevents any such mass mixing through the Higgs portal. In this scenario, the second Higgs doublet being Z_2 odd does not couple to fermions. Moreover, we get two CP even neutral Higgs bosons h and H_0 , where h is identified as the SM-like Higgs boson of mass 125 GeV which is discovered at the LHC. We also get one pseudoscalar Higgs boson A and a pair of charged Higgs bosons H^\pm . Notice from Eq. (2.6) that the heavy Higgs bosons H_0 , A and H^\pm from second doublet are nearly degenerate. Depending upon the sign of λ_5 one of the scalars between A and H_0 can be the lightest, and hence can be a cold DM candidate. Since all the physical Higgs bosons except h are Φ_2 -type, i.e., Z_2 -odd, this will also restrict their decay modes.

2.2 The Type-III and Inverse Seesaw Lagrangians

In addition to the SM particle contents, the Type-III seesaw model contains $SU(2)_L$ fermionic triplets Σ with zero hypercharge. Being in the adjoint representation of the $SU(2)_L$ group, the Majorana mass term M_N of such triplets is gauge invariant. In terms of the usual two-by-two notation for triplets, the beyond SM interactions are described by the Lagrangian:

$$\mathcal{L}_{\text{III}} = Tr[\bar{\Sigma} i \not{D} \Sigma] - \frac{1}{2} Tr[\bar{\Sigma} M_N \Sigma^c + \bar{\Sigma}^c M_N^* \Sigma] - \sqrt{2}(\tilde{\Phi}_1^\dagger \bar{\Sigma} Y_N L + \bar{L} Y_N^\dagger \Sigma \tilde{\Phi}_1), \quad (2.7)$$

where $L \equiv (\nu, \ell)_L$ is the SM lepton doublet, $\tilde{\Phi}_1 = i\sigma_2 \Phi_1^*$ (with σ_2 being the second Pauli matrix), $\Sigma^c \equiv C \bar{\Sigma}^T$ for each fermionic triplet as shown below.

$$\Sigma = \begin{pmatrix} \Sigma^0/\sqrt{2} & \Sigma^+ \\ \Sigma^- & -\Sigma^0/\sqrt{2} \end{pmatrix}, \quad \Sigma^c = \begin{pmatrix} \Sigma^{0c}/\sqrt{2} & \Sigma^{-c} \\ \Sigma^{+c} & -\Sigma^{0c}/\sqrt{2} \end{pmatrix}$$

We drop the generation indices here, but this is to remind that there are three set of fermionic triplets for three leptonic doublets. The covariant derivative generates the coupling between the W bosons and the triplet fermions and they are proportional to g_2 as shown below,

$$\not{D}_\mu = \not{\partial}_\mu - i\sqrt{2}g_2 \begin{pmatrix} W_\mu^3/\sqrt{2} & W_\mu^+ \\ W_\mu^- & -W_\mu^3/\sqrt{2} \end{pmatrix}.$$

Without loss of generality, we start from the basis, where M_N is real and diagonal. In order to consider the mixing of fermionic triplets with the charged leptons, it is convenient to express the four degrees of freedom of each charged triplet in terms of a single Dirac spinor:

$$\psi = \Sigma_R^{+c} + \Sigma_R^- . \quad (2.8)$$

On the other hand the neutral fermionic triplet components can be left in two-component notation, since they have only two degrees of freedom and mix with neutrinos, which are also described by two-component fields. This leads to the Lagrangian as follows

$$\begin{aligned} \mathcal{L}_{\text{III}} = & \bar{\psi} i \not{\partial} \psi + \bar{\Sigma}_R^0 i \not{\partial} \Sigma_R^0 - \bar{\psi} M_N \psi - \left(\bar{\Sigma}_R^0 \frac{M_N}{2} \Sigma_R^{0c} + h.c. \right) \\ & + g \left(W_\mu^+ \bar{\Sigma}_R^0 \gamma_\mu P_R \psi + W_\mu^+ \bar{\Sigma}_R^{0c} \gamma_\mu P_L \psi + h.c. \right) - g W_\mu^3 \bar{\psi} \gamma_\mu \psi \\ & - \left(\Phi^0 \bar{\Sigma}_R^0 Y_N \nu_L + \Phi^+ \bar{\Sigma}_R^0 Y_N \ell_L + \sqrt{2} (\Phi^0 \bar{\psi} Y_N \ell_L - \Phi^+ \bar{\nu}_L^c Y_N^T \psi) + h.c. \right). \end{aligned} \quad (2.9)$$

The mass term of the charged sector shows the usual aspect for Dirac particles:

$$\mathcal{L} \ni - (\bar{l}_R \ \bar{\psi}_R) \begin{pmatrix} m_l & 0 \\ Y_N v & M_N \end{pmatrix} \begin{pmatrix} l_L \\ \psi_L \end{pmatrix} - (\bar{l}_L \ \bar{\psi}_L) \begin{pmatrix} m_l & Y_N^\dagger v \\ 0 & M_N \end{pmatrix} \begin{pmatrix} l_R \\ \psi_R \end{pmatrix},$$

where $m_\ell = y_\ell < \phi^0 >$ with y_ℓ is leptonic Yukawa coupling and $v = \sqrt{2} < \phi^0 > = 246$ GeV. On the other hand the symmetric mass matrix for the neutral states is given by

$$\begin{aligned} \mathcal{L} \ni & - (\bar{\nu}_L \ \bar{\Sigma}^{0c}) \begin{pmatrix} 0 & Y_N^\dagger v / 2\sqrt{2} \\ Y_N^* v / 2\sqrt{2} & M_N / 2 \end{pmatrix} \begin{pmatrix} \nu_L^c \\ \Sigma^0 \end{pmatrix} \\ & - (\bar{\nu}_L^c \ \bar{\Sigma}^0) \begin{pmatrix} 0 & Y_N^T v / 2\sqrt{2} \\ Y_N v / 2\sqrt{2} & M_N / 2 \end{pmatrix} \begin{pmatrix} \nu_L \\ \Sigma^{0c} \end{pmatrix}. \end{aligned}$$

The neutrino mass matrix in this case can be written as

$$\mathcal{M}_\nu = \begin{pmatrix} 0 & M_D \\ M_D^T & M_N \end{pmatrix} \quad \text{where} \quad M_D = \frac{v}{\sqrt{2}} Y_N. \quad (2.10)$$

Thus the light neutrino mass can be written as

$$m_\nu = -\frac{v^2}{2} Y_N^T \frac{1}{M_N} Y_N, \quad (2.11)$$

which mixes the left-handed neutrinos and the neutral fermionic triplet components (right-handed neutrinos). This leads to the full mass matrix for the neutral states as:

$$\mathcal{M}_\nu = \begin{pmatrix} 0 & M_D \\ M_D^\top & M_N \end{pmatrix}. \quad (2.12)$$

After block diagonalization and in the seesaw limit $\|M_D\| \ll \|M_N\|$, we obtain the mass eigenvalues for the light neutrinos as

$$m_\nu \simeq -M_D M_N^{-1} M_D^\top, \quad (2.13)$$

whereas the neutral fermionic triplet mass eigenstates have masses of order M_N . From Eq. (2.13), it is clear that in order to have the correct order of magnitude of light neutrino mass $m_\nu \lesssim 0.1$ eV, as required by the oscillation data as well as the cosmological constraints, the Yukawa couplings in the canonical seesaw have to be very small, unless the neutral triplet components are super heavy. For instance, for $M_N \sim \mathcal{O}(100 \text{ GeV})$, we require $Y_N \lesssim \mathcal{O}(10^{-6})$. We will see later that these coupling values are too small to have any impact in the RG evolution of other couplings, and thus, the neutral triplet components in the canonical seesaw have effectively no contribution to the vacuum stability in this model.

The collider signatures of heavy neutrinos and lepton rely upon larger Yukawa couplings. These are further restricted from electroweak precision data [73–77]. In the inverse seesaw frame work [78–81], we introduce another set of fermions which are $SU(2)_L$ triplet, Σ_{2i} (with $i = 1, 2, 3$) along with the Σ_{1i} . The corresponding Yukawa Lagrangian is given by

$$\begin{aligned} \mathcal{L}_{\text{ISS}} = & Tr[\overline{\Sigma_{1i}} \not{D} \Sigma_{1i}] + Tr[\overline{\Sigma_{2i}} \not{D} \Sigma_{2j}] - \frac{1}{2} Tr[\overline{\Sigma_{2i}} \mu_{\Sigma_{ij}} \Sigma_{2j}^c + \overline{\Sigma_{2i}^c} \mu_{\Sigma_{ij}}^* \Sigma_{2j}] \\ & - \left(\tilde{\Phi}_1^\dagger \overline{\Sigma_{1i}} \sqrt{2} Y_{N_{ij}} L_j + Tr[\overline{\Sigma_{1i}} M_{N_{ij}} \Sigma_{2j}] + \text{H.c.} \right), \end{aligned} \quad (2.14)$$

where M_N is a 3×3 Dirac mass matrix in the triplet sector and μ_S is the small lepton number breaking mass term for the Σ_2 -fields. In the basis of $\{\nu_L^c, \Sigma_1^0, \Sigma_2^0\}$, the full 9×9 neutral components mass matrix takes the form

$$\mathcal{M}_\nu = \begin{pmatrix} 0 & M_D & 0 \\ M_D^\top & 0 & M_N \\ 0 & M_N^\top & \mu_\Sigma \end{pmatrix}. \quad (2.15)$$

After diagonalization of the mass matrix Eq. (2.15) one obtains the three light neutrino masses

$$m_\nu \simeq M_D M_N^{-1} \mu_\Sigma (M_N^\top)^{-1} M_D^\top, \quad (2.16)$$

whereas the remaining six mass eigenstates are mostly sterile states with masses given by $M_N \pm \mu_\Sigma/2$. Here the presence of additional fermionic triplet and the extra mass term μ_Σ give us the freedom to accommodate any M_N values while having sizable Yukawa couplings.

Irrespective of the underlying model framework, if we take large $Y_N \sim \mathcal{O}(1)$, it will have a significant negative contribution to the running of quartic couplings via the ISS at scales $\mu > M_N$ [82]. This must be taken into account in the study of EW vacuum stability in low-scale seesaw scenarios, as we shown below.

3 Perturbativity

To illustrate the theoretical bounds from perturbativity behaviour of the dimensionless couplings, we impose that the dimensionless couplings of the model must remain perturbative for a given value of the energy scale μ , i.e. the couplings must satisfy the following constraints:

$$|\lambda_i| \leq 4\pi, \quad |g_j| \leq 4\pi, \quad |Y_k| \leq \sqrt{4\pi}, \quad (3.1)$$

where λ_i with $i = 1, 2, 3, 4, 5$ are the scalar quartic couplings; g_j with $j = 1, 2$ are EW gauge couplings;¹ and Y_k with $k = u, d, \ell$ are all Yukawa couplings for the up, down type quarks and leptons respectively. The extension of SM with a $SU(2)_L$ inert doublet as well as by $SU(2)_L$ triplet fermions can change the running $g_2(\mu)$, which in turn affects the progression of other couplings namely the λ_i relevant for the vacuum stability and perturbativity. Below we discuss that how $g_2(\mu)$ gets affected via the extra scalar and fermions of this model.

3.1 Running of Gauge couplings:

Eqs. 3.2- 3.4 and Figure 1(c) describe the evolution of the SM gauge couplings at a given scale μ (not explicitly mentioned in those Eqs.) at two-loop level. Both g_2 and g_3 decrease with the increase in the running scale μ and remain perturbative in the high scale limit. However, such behaviour can change substantially with the inclusion of other $SU(2)_L$ fields such as ID and Type-III Seesaw fermions, which are in the triplet of $SU(2)_L$ representation.

¹The running of the strong coupling g_3 is same as in the SM, so we do not show it here.

$$\beta_{g_1} = \frac{1}{16\pi^2} \left[\frac{21}{5} g_1^3 \right] + \frac{1}{(16\pi^2)^2} \left[\frac{1}{50} g_1^3 (180g_2^2 + 208g_1^2 - 25\text{Tr}(Y_d Y_d^\dagger)) \right. \\ \left. + 440g_3^2 - 45\text{Tr}(Y_N Y_N^\dagger) - 75\text{Tr}(Y_e Y_e^\dagger) - 85\text{Tr}(Y_u Y_u^\dagger) \right], \quad (3.2)$$

$$\beta_{g_2} = \frac{1}{16\pi^2} \left[-\frac{19}{6} g_2^3 \right] + \frac{1}{(16\pi^2)^2} \left[\frac{1}{30} g_2^3 (-15\text{Tr}(Y_e Y_e^\dagger) + 175g_2^2 + 27g_1^2 \right. \\ \left. + 360g_3^2 - 45\text{Tr}(Y_d Y_d^\dagger) - 45\text{Tr}(Y_u Y_u^\dagger) \right], \quad (3.3)$$

$$\beta_{g_3} = \frac{1}{16\pi^2} \left[-7g_3^3 \right] + \frac{1}{(16\pi^2)^2} \left[-\frac{1}{10} g_3^3 (-11g_1^2 + 20\text{Tr}(Y_d Y_d^\dagger)) \right. \\ \left. + 20\text{Tr}(Y_u Y_u^\dagger) + 260g_3^2 - 45g_2^2 \right]. \quad (3.4)$$

In Eq. 3.5-Eq. 3.9, we show the modified evolution of the gauge couplings in the presence of the ID and triplet fermions. Eq. 3.5 shows that an inclusion of inert $SU(2)_L$ doublet makes β_{g_2} less negative at one-loop and so as at two-loop. The behaviours can be verified from the Figure 1(a), where the blue curve implies SM and green line represents SM with ID. For the comparison we also show that an addition of a $Y = 0$ $SU(2)_L$ triplet scalar also reduces the negative impact in β_{g_2} , as can be read from Eq. 3.6, which is also evident from Figure 1(a) orange curve. However, from Eq. 3.7 we can see that even at one-loop β_{g_2} has become positive with the factor changed to $\frac{5g_2^3}{6}$ if we extend the SM with three generations of Type-III fermions. This behaviour continues even at two-loop. The running of g_2 in this case has been depicted by red curve of Figure 1(a). Unlike the SM, or ID scenario, the coupling g_2 in this case increases with increasing μ . In addition to the three generations of Type-III fermions if we add a $SU(2)_L$ inert doublet which gives the much needed DM candidate, the factor at one-loop is enhanced to $5g_2^3$ with further enhancement at two-loop and also visible by the sky-blue curve in Figure 1(a). Certainly we can see such models loses perturbativity of the gauge coupling around much lower value of the running scale, i.e., $\mu \lesssim 10^{10}$ GeV. However, restricting to two generations of triplet fermions, and one ID, this scale pushes even after the GUT scale $\mu \sim 10^{17}$ GeV. This prompt us to choose only two generations of Type-III fermions along with ID, rather than the three generations. The running of the gauge coupling g_2 for the two generation scenario is evident from the purple curve of Figure 1(a), and also from Eq. 3.9. Figure. 1(b) represents running of all the three gauge couplings for the two generation scenario. Therefore, SM extension with an ID and two generations of Type-III fermions with ISS mechanism are more motivated, as this accommodates

perturbativity of the gauge couplings above the GUT scale, as well as, can explain two small light neutrino masses, and provide a dark matter candidate from the ID.

$$\beta_{g_2^{IDM}} = \frac{1}{16\pi^2} \left[-3g_2^3 \right] + \frac{1}{(16\pi^2)^2} \left[\frac{1}{10}g_2^3 \left(120g_3^2 + 12g_1^2 - 15\text{Tr}(Y_d Y_d^\dagger) \right. \right. \\ \left. \left. - 15\text{Tr}(Y_u Y_u^\dagger) - 5\text{Tr}(Y_e Y_e^\dagger) + 80g_2^2 \right) \right]. \quad (3.5)$$

$$\beta_{g_2^{TM}} = \frac{1}{16\pi^2} \left[-\frac{17}{6}g_2^3 \right] + \frac{1}{(16\pi^2)^2} \left[\frac{1}{30}g_2^3 \left(-15\text{Tr}(Y_e Y_e^\dagger) + 27g_1^2 + 360g_3^2 \right. \right. \\ \left. \left. + 455g_2^2 - 45\text{Tr}(Y_d Y_d^\dagger) - 45\text{Tr}(Y_u Y_u^\dagger) \right) \right]. \quad (3.6)$$

$$\beta_{g_2, 3gen}^{Type-III} = \frac{1}{16\pi^2} \left[\frac{5}{6}g_2^3 \right] + \frac{1}{(16\pi^2)^2} \left[\frac{1}{60}g_2^3 \left(-165\text{Tr}(Y_e Y_e^\dagger) - 30\text{Tr}(Y_e Y_e^\dagger) \right. \right. \\ \left. \left. + 4190g_2^2 + 54g_1^2 + 720g_3^2 - 90\text{Tr}(Y_d Y_d^\dagger) - 90\text{Tr}(Y_u Y_u^\dagger) \right) \right], \quad (3.7)$$

$$\beta_{g_2, 3gen} = \frac{1}{16\pi^2} \left[5g_2^3 \right] + \frac{1}{(16\pi^2)^2} \left[\frac{1}{10}g_2^3 \left(120g_3^2 + 12g_1^2 + 1360g_2^2 - 15\text{Tr}(Y_d Y_d^\dagger) \right. \right. \\ \left. \left. - 15\text{Tr}(Y_u Y_u^\dagger) - 55\text{Tr}(Y_N Y_N^\dagger) - 5\text{Tr}(Y_e Y_e^\dagger) \right) \right], \quad (3.8)$$

$$\beta_{g_2, 2gen} = \frac{1}{16\pi^2} \left[\frac{7}{3}g_2^3 \right] + \frac{1}{(16\pi^2)^2} \left[\frac{1}{30}g_2^3 \left(-15\text{Tr}(Y_e Y_e^\dagger) - 165\text{Tr}(Y_N Y_N^\dagger) \right. \right. \\ \left. \left. + 2800g_2^2 + 360g_3^2 + 36g_1^2 - 45\text{Tr}(Y_d Y_d^\dagger) - 45\text{Tr}(Y_u Y_u^\dagger) \right) \right]. \quad (3.9)$$

The perturbative nature of the scalar quartic couplings are also modified by the inclusion of ID and triplet fermions. Below, we first focus on the analysis of the perturbative behaviour of the scalar quartic couplings with respect to λ_3 in the scenario with SM associated with an ID, and three generations of fermionic triplet. The perturbative limit is calculated if at least one of the coupling crosses the perturbativity or hits Landau pole. Figure 2 describes the perturbative behaviour of λ_3 with the scale μ for $Y_N = 0.02$, where the other quartic couplings $\lambda_{(i=2,4,5)}$ are kept at different values at the electroweak scale. For the coupling λ_1 , we choose $\lambda_1 = 0.1264$, which gives SM like Higgs boson mass around 125.5 GeV. Here red, green, blue and purple curves in each plot correspond to $\lambda_i, i = 2, 4, 5$ at the EW scale, representative of very weak ($\lambda_i = 0.01$), weak ($\lambda_i = 0.10$), moderate ($\lambda_i = 0.40$) and strong ($\lambda_i = 0.80$) coupling limits, respectively.

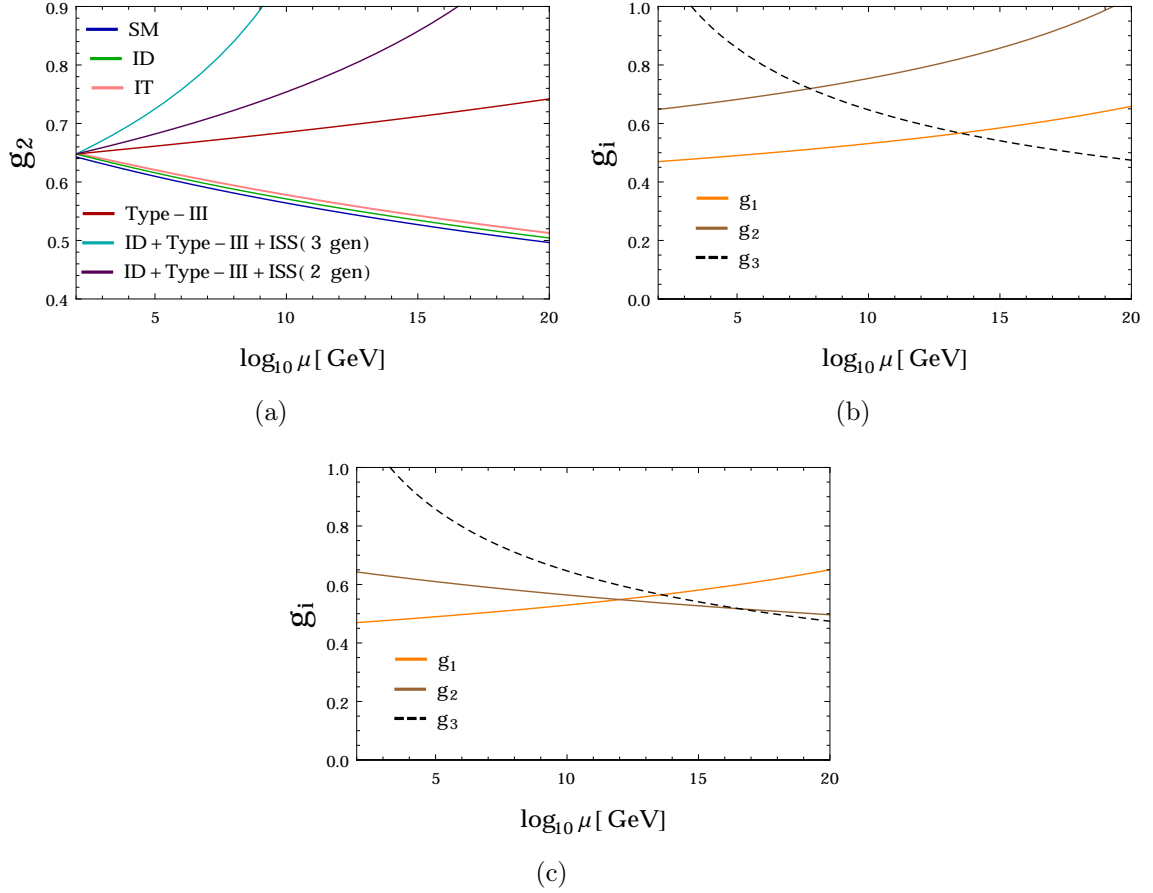


Figure 1. (a) Running of g_2 with the scale μ for the SM in blue, SM + ID in green, SM + ITM in pink, SM + three generations of Type-III fermions in red, SM+ID + three generations of Type-III fermions in sky-blue and SM+ ID+ two generations of Type-III fermions in purple in two-loop. (b) Running of all three gauge couplings g_i at two-loop for the SM+ ID+ two generations of Type-III fermions. (c) Running of all three gauge couplings g_i at two-loop for the SM.

In ID+Type-III+ ISS scenario we have three generations of fermionic triplet Σ_{1i} which generates the Dirac term and three generations of additional fermionic triplet Σ_{2j} instrumental for inverse seesaw mechanism. Having $SU(2)_L$ charge they contribute to the beta functions of the $SU(2)_L$ gauge coupling, i.e. β_{g_2} positively; which is somewhat different than normal Type-I + ISS case [19]. Additionally Y_N also contributes positively to the beta functions of $\lambda_{3,4,5}$ at one-loop and negative effects only comes at two-loop. Both Y_N and β_{g_2} push the $\lambda_{3,4,5}$ towards non-perturbative limit. The Higgs quartic couplings λ_1 get negative corrections from the Yukawa coupling Y_N , pushing the Higgs potential toward instability at one-loop and two-loop. The detailed two-loop beta functions are given in Appendix A, where only two generation effects are shown. However, in Figure 2 we have considered all three generations

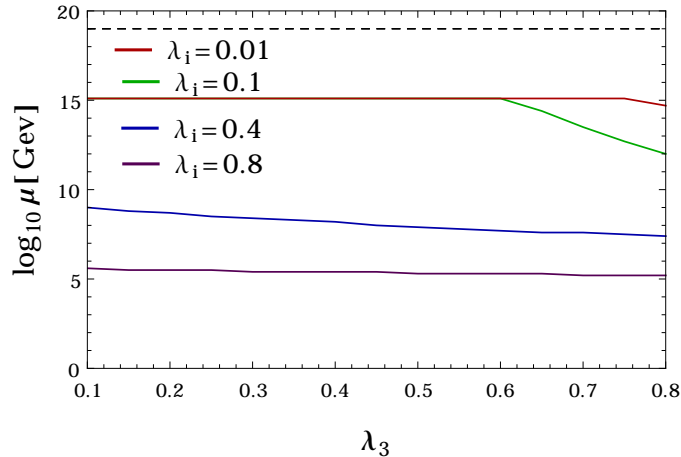


Figure 2. Two-loop running of the scalar quartic coupling λ_3 as a function of perturbative scale for Yukawa coupling $Y_N = 0.02$, considering three generations of fermionic triplet. Here red, green, blue and purple curves correspond to different initial conditions for λ_i (with $i = 2, 4, 5$) at the EW scale. The different lines represent $\lambda_i = 0.01, 0.1, 0.4, 0.8$ respectively.

of $SU(2)_L$ triplet fermions along with ID which makes the theory more stable, but simultaneously becomes non-perturbative below Planck scale for all corresponding values of λ_i and Y_N . Thus for the Planck scale perturbativity we should restrict ourselves to two generations of fermionic triplets. For $\lambda_i = 0.01, 0.10$ which is less than $\lambda_1 = 0.1264$, λ_1 hits Landau pole before going into instability around 10^{15} GeV (red and green lines). This happens due to positive effect of g_2 , which is different than the Type-I case [19]. The bending happens due to further positive effects of $\lambda_1 \text{Tr}(Y_N^\dagger Y_N)$ and other quadratic terms involving λ_i s. Such bending effects grows from $\lambda_i = 0.01$ (brown line) to $\lambda_i = 0.10$ (green line). For $\lambda_i \geq 0.2$ the perturbative limits come at much smaller case as other λ_i s hit the Landau pole before λ_1 .

In Figure 3, we present the perturbative behaviour of the Higgs quartic couplings for SM extension with ID + Type-III + ISS with two generations of fermionic triplets. The perturbativity behaviour of the scalar quartic couplings $\lambda_{3,4,5}$ are studied in Figure 3(a) - 3(f) respectively for two different choices of the coupling Y_N , i.e. $Y_N = 0.01, 0.40$. The other quartic couplings λ_i are chosen to be 0.01, 0.1, 0.4 and 0.8 which are shown by the red, green, blue and purple lines, respectively. Higgs quartic coupling λ_3 is perturbative till Planck scale for $\lambda_3 \lesssim 0.56, 0.37$ for $\lambda_i(\text{EW}) = 0.01, 0.10$ respectively, as shown in Figure 3(a). For a larger coupling $\lambda_i(\text{EW}) = 0.40, 0.80$ theory becomes non-perturbative at much lower scale $\sim 10^{8.9}, 10^{5.7}$ GeV for almost all initial values of λ_3 , and for a coupling $Y_N = 0.01$. Figure 3(b) shows the similar behaviour of λ_3 for a larger Y_N , where we choose $Y_N = 0.40$ and the other quartic couplings $\lambda_i(\text{EW}) = 0.01, 0.10$. As is evident from Figure 3(b), the Higgs

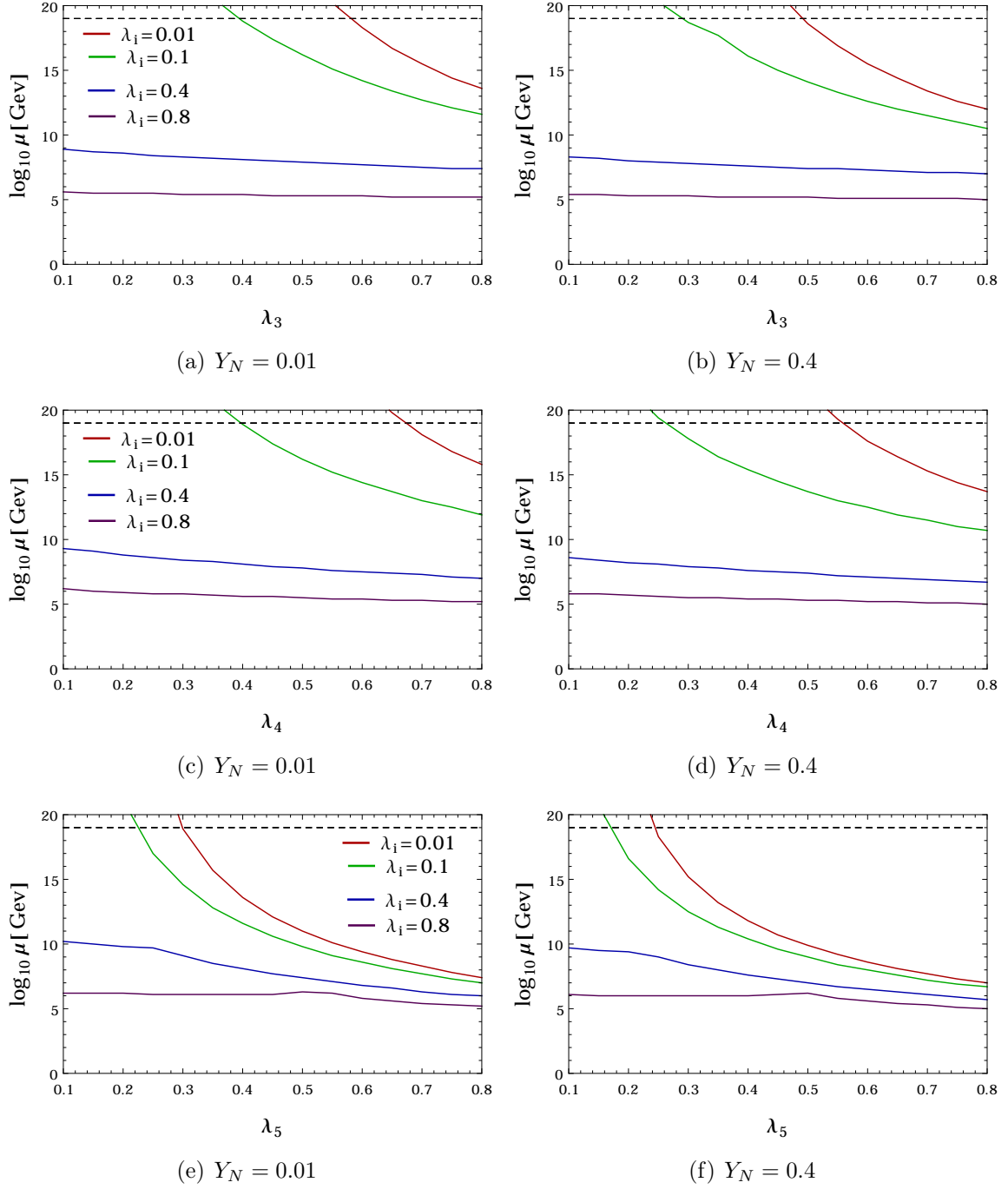


Figure 3. Perturbative limits of λ_3 , λ_4 and λ_5 for various λ_i s and $Y_N = 0.01, 0.40$. Here red, green, blue and purple curves in each plot correspond to λ_i for the running of λ_3 , λ_4 and λ_5 at the EW scale, representative of very weak ($\lambda_i = 0.01$), weak ($\lambda_i = 0.1$), moderate ($\lambda_i = 0.4$) and strong ($\lambda_i = 0.8$) coupling respectively. Here, we consider two generations of fermionic triplet in the SM plus ID plus Type-III ISS scenario.

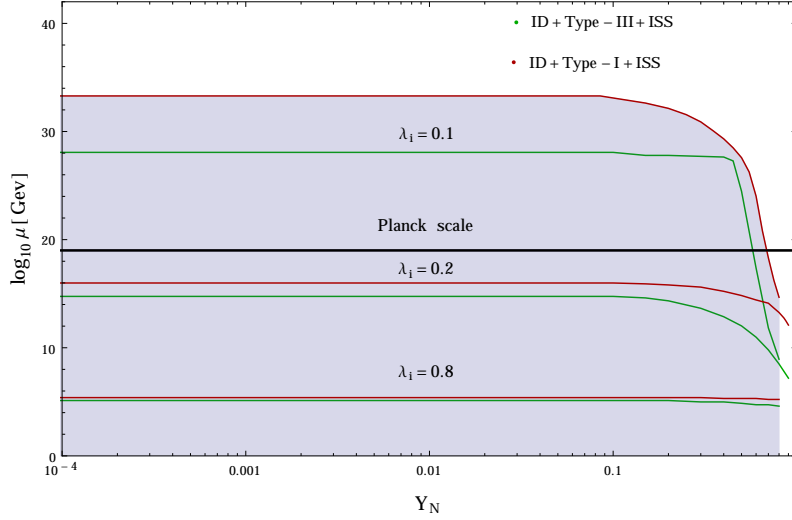


Figure 4. Bounds from perturbativity on Y_N as a function of μ for different values of λ_i with $y_t = 0.9369$, $M_N = 100$ GeV. The red curve and the green curve corresponds to the ID plus Type-I ISS scenario and ID plus Type-III ISS scenario respectively with two generations of fermionic triplets.

quartic coupling λ_3 is perturbative till Planck scale for $\lambda_3 \lesssim 0.47, 0.26$ for the above choices of $\lambda_i(\text{EW})$. For $\lambda_i(\text{EW}) = 0.40, 0.80$, theory again becomes non-perturbative at much lower scale $\sim 10^{8.4}, 10^{5.4}$ GeV for almost all initial values of λ_3 . Similarly, the perturbative bounds on Higgs quartic coupling λ_4 are shown in Figure 3(c)-3(d). The results are very similar to the case of λ_3 . Here for the choice of $\lambda_i(\text{EW}) = 0.01, 0.10$ the perturbative limits remain valid till the Planck scale for $\lambda_4 \lesssim 0.64, 0.36$ and for $Y_N = 0.01$. For a larger $Y_N = 0.40$, the corresponding perturbative limit turns out to be $\lambda_4 \lesssim 0.54, 0.24$. For higher values of $\lambda_i(\text{EW})$, theory becomes non-perturbative at much lower scale, i.e. $\sim 10^{9.2}, 10^{6.1}$ GeV for $Y_N = 0.01$ and $\sim 10^{8.8}, 10^{5.9}$ GeV for almost all initial values of λ_4 and for the choice of Yukawa couplings $Y_N = 0.01$ and $Y_N = 0.40$, respectively. As depicted in Figure 3(e)- 3(f), Higgs quartic coupling λ_5 is perturbative till Planck scale for $\lambda_5 \lesssim 0.29, 0.22$ for $Y_N = 0.01$ and $\lambda_5 \lesssim 0.24, 0.16$ for $Y_N = 0.40$ for the choice of $\lambda_i(\text{EW}) = 0.01, 0.10$ respectively. For higher values of $\lambda_i(\text{EW})$, theory becomes non-perturbative at much lower scale $\sim 10^{10.1}, 10^{6.2}$ GeV for $Y_N = 0.01$ and $\sim 10^{9.8}, 10^{6.1}$ GeV for $Y_N = 0.40$ respectively for almost all initial values of λ_5 . The perturbative scale decreases for larger choices of Y_N as $\lambda_{3,4,5}$ increases with Y_N and even faster than Type-I case [19] with the stringent constraint comes from the perturbativity bound of λ_5 . Here the theory becomes non-perturbative before Planck scale for $\lambda_i(\text{EW}) = 0.40, 0.80$ respectively. For $\lambda_i(\text{EW}) = 0.01, 0.10$ the Planck scale validity can be achieved for $\lambda_5 \leq 0.30, 0.22$ and $\lambda_5 \leq 0.25, 0.17$ for the choices of $Y_N = 0.01, 0.40$ respectively.

Figure 4 shows the bounds on Yukawa coupling Y_N from perturbativity of λ_i for different initial $\lambda_{(i=2,3,4,5)}$ values. Even if we allow for Y_N values up to 0.1, the effect of triplet fermions on the perturbativity of λ_i is hardly noticeable as shown in Figure 4. The exact value of Y_N where it starts affecting the perturbativity depends on the initial value of λ_i . However, due to enhance g_2 in the case of Type-III, λ_i attains perturbation limit before than Type-I case and the effect is more prominent for lower values of $\lambda_i(\text{EW})$. For $\lambda_i(\text{EW}) = 0.1$ in ID+Type-III+ISS, the λ_1 hits Landau pole before other λ s as $\lambda_1(\text{EW}) = 0.1264$ and gets large positive contribution from the enhanced g_2 in this case. Effects of other λ_i s are negligible in this case until a particular value of Y_N . Large g_2 effect brings the perturbative scale to $10^{28.07}$ GeV with prolonged effect till $Y_N \lesssim 0.23$ after which $\lambda_1 \text{Tr}(Y_N^\dagger Y_N)$ effect takes over bringing perturbative scale further down as can be seen from the green line with the bending effect. Compared to that in ID+Type-I+ISS case, for $\lambda_i = 0.1$, the perturbativity scale is $\sim 10^{33.29}$ GeV and the effect starts showing up for $Y_N > 0.15$ in ID+Type-I+ISS as can be seen in red line. Here perturbative limits are obtained via the Landau poles of other λ_i as g_2 decreases with the scale in this case and large Y_N pushes λ_1 towards negative values of instability [19]. However, other λ_i gets positive contributions $\lambda_i \text{Tr}(Y_N^\dagger Y_N)$ towards their Landau pole. Like the Type-III case here also being very small λ_i effects are negligible.

For higher values of $\lambda_i(\text{EW})$, the perturbativity limits are obtained when other λ s hit Landau pole before λ_1 and mostly controlled by λ_i (see Appendix A) and λ_1 runs towards instability by large Y_N effect. This also results in lesser splitting in the perturbative scale between Type-III and Type-I until $\lambda_i \text{Tr}(Y_N^\dagger Y_N)$ effects creep in with larger factor for Type-III as compared to Type-I. For $\lambda_i = 0.2$, the perturbativity limit is constant around the GUT scale 10^{16} , 10^{15} GeV and the fermion effect starts for $Y_N \gtrsim 0.3$ in both scenarios but the effect of Y_N is much stronger in ID+Type-III+ISS.

For further higher values of $\lambda_i = 0.8$, the perturbativity scales are almost the same $\sim 10^5$ GeV for both Type-I and Type-III cases mostly governed by the λ_i effects. The effect of new fermion comes much later for $Y_N > 0.60$. Higher values of λ_i s can accommodate higher values of Y_N for vacuum stability in λ_1 direction, but on the contrary, they make the theory non-perturbative at much lower scale. We infer from Figure 4 that an upper bound comes from perturbativity on λ_i and Y_N values, i.e. $\lambda_i \leq 0.15$ and $Y_N \leq 0.25$, $Y_N \leq 0.3$ the theory to remains perturbative till the Planck scale for Type-III and Type-I respectively.

4 Stability Bound

In this section we analyse the stability of Higgs potential via two different approaches. Firstly via calculating two-loop scalar quartic couplings and checking if the SM Higgs like quartic coupling λ_h becomes negative at some higher scale. In this case $\lambda_h = \lambda_1$ at

tree-level, but at one-loop and two-loop levels λ_h gets contribution from SM fields as well as the ID and the Type-III fermions. The details are provided in subsection 4.1. For simplicity, we only present the expressions of the corresponding beta functions at one-loop in the next subsection. The expressions for the two-loop beta functions are given in the Appendix A. Secondly we follow the effective potential approach as described in detail in section 4.3.

4.1 RG Evolution of the Scalar Quartic Couplings

To study the evaluations of dimensionless couplings we have implemented the ID + Type-III Seesaw + ISS scenario in SARAH 4.13.0 [83] for two generations $SU(2)_L$ triplet fermions. The corresponding β -functions for various gauge, quartic and Yukawa couplings are calculated at one- and two-loop levels. The explicit expressions for the two-loop β -functions can be found in Appendix A, and they have been used in our numerical analysis of vacuum stability in this section. To illustrate the effect of the Yukawa and additional scalar quartic couplings on the RG evolution of the SM-like Higgs quartic coupling λ_1 in the scalar potential (2.3), let us first look at the one-loop β -functions. $\lambda_h = \lambda_1$ at tree-level and at the one-loop level, the β -function for the SM Higgs quartic coupling in this model receives three different types of contributions: one from the SM gauge, Yukawa, quartic interactions, the second from the Type-III Seesaw Yukawa couplings, and the third from the inert scalar sector (ID):

$$\beta_{\lambda_h} = \beta_{\lambda_1} = \beta_{\lambda_1}^{\text{SM}} + \beta_{\lambda_1}^{\text{Type-III+ISS}} + \beta_{\lambda_1}^{\text{ID}}, \quad (4.1)$$

with

$$\begin{aligned} \beta_{\lambda_1}^{\text{SM}} = & \frac{1}{16\pi^2} \left[\frac{27}{200}g_1^4 + \frac{9}{20}g_1^2g_2^2 + \frac{9}{8}g_2^4 - \frac{9}{5}g_1^2\lambda_1 - 9g_2^2\lambda_1 + 24\lambda_1^2 \right. \\ & + 12\lambda_1\text{Tr}(Y_uY_u^\dagger) + 12\lambda_1\text{Tr}(Y_dY_d^\dagger) + 4\lambda_1\text{Tr}(Y_eY_e^\dagger) \\ & - 6\text{Tr}(Y_uY_u^\dagger Y_uY_u^\dagger) - 6\text{Tr}(Y_dY_d^\dagger Y_dY_d^\dagger) \\ & \left. - 2\text{Tr}(Y_eY_e^\dagger Y_eY_e^\dagger) \right], \end{aligned} \quad (4.2)$$

$$\beta_{\lambda_1}^{\text{Type-III+ISS}} = \frac{1}{16\pi^2} \left[12\lambda_1\text{Tr}(Y_NY_N^\dagger) - 10\text{Tr}(Y_NY_N^\dagger Y_NY_N^\dagger) \right], \quad (4.3)$$

$$\beta_{\lambda_1}^{\text{ID}} = \frac{1}{16\pi^2} \left[2\lambda_3^2 + 2\lambda_3\lambda_4 + \lambda_4^2 + 4\lambda_5^2 \right]. \quad (4.4)$$

Here g_1, g_2 are respectively the $U(1)_Y, SU(2)_L$ gauge couplings, and Y_u, Y_d, Y_e are respectively the up, down and electron-type Yukawa coupling matrices in the SM. We use the SM input values for these parameters at the EW scale [41]: $\lambda_1 = 0.1264$, $g_1 = 0.3583$, $g_2 = 0.6478$, $y_t = 0.9369$ and other Yukawa couplings are neglected [9]. It is

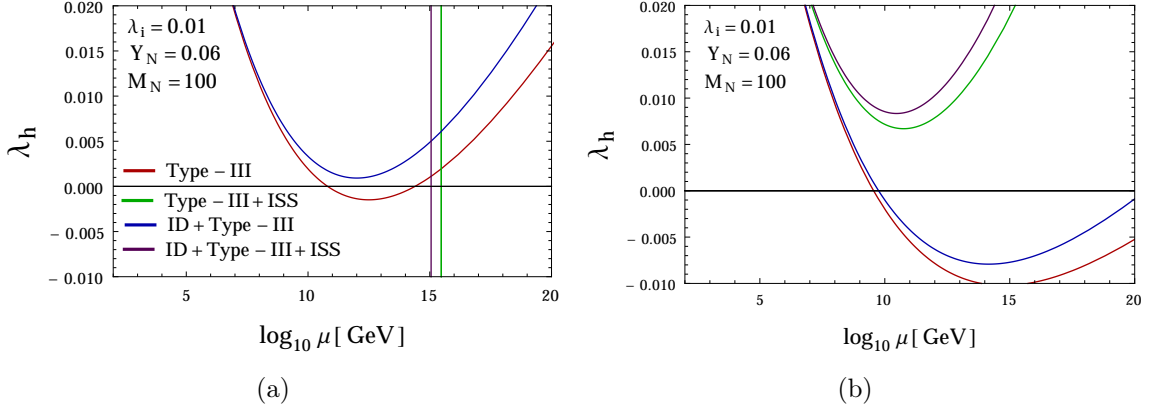


Figure 5. Two loop running of the SM like Higgs quartic coupling as a function of energy. Here the red, green, blue and the purple curve correspond to the Type-III Seesaw, Type-III Seesaw+ISS, ID+Type-III Seesaw and ID+Type-III Seesaw+ISS scenarios. The left and right plot represent three generations and two generations of fermionic triplets, respectively.

important to note that the ISS contribution to the RG evolution of λ_1 is applicable only above the threshold of M_N .

In Figure 5(a)-5(b), we show the respective λ_h running with the scale μ . The plot in the left panel represents the three generation scenario, and the plot in the right panel represents two generations scenario. The two plots describe the behaviour of λ_h at two-loop level for four different cases as before with three and two generations of triplet fermions, where $M_N = 100$ GeV, $\lambda_1 = 0.1264$, $\lambda_i = 0.01$ (with $i = 2, 3, 4, 5$) at the EW scale. The RG evolution of the SM Higgs quartic coupling $\lambda_1 \equiv \lambda_h$ as a function of the energy scale μ are shown where the red curve shows the RG evolution of λ_h using $\beta_{\lambda_1}^{\text{SM}} + \beta_{\lambda_1}^{\text{Type-III}}$ only, while the green curve shows the evolution using $\beta_{\lambda_1}^{\text{SM}} + \beta_{\lambda_1}^{\text{Type-III}} + \beta_{\lambda_1}^{\text{ISS}}$, blue curve describes the evolution using $\beta_{\lambda_1}^{\text{SM}} + \beta_{\lambda_1}^{\text{Type-III}} + \beta_{\lambda_1}^{\text{ID}}$, and finally the purple curve shows the full evolution using $\beta_{\lambda_1} \equiv \beta_{\lambda_1}^{\text{SM}} + \beta_{\lambda_1}^{\text{Type-III}} + \beta_{\lambda_1}^{\text{ISS}} + \beta_{\lambda_1}^{\text{ID}}$ [cf. Eq. (4.1)]. The added effects of the new contributions to $\lambda_1 \equiv \lambda_h$ at one-loop are given in Eq. (4.1) and the detailed two-loop expressions are written in Appendix A.

In Figure 5(a), the three generations of fermionic triplet make the g_2 contribution too large (see Eq. 3.8) for both Type-III+ISS (green) and ID+ Type-III +ISS (purple), such that β_{λ_1} hits the Landau pole at $\sim 10^{15.4}$ GeV and $\sim 10^{15.1}$ GeV respectively before hitting the instability scale (at which $\lambda_h \leq 0$). This makes the theory non-perturbative below Planck scale. Without ISS the β_{g_2} is relatively smaller (see subsection 3.1) which restrains λ_h from hitting the Landau pole. Thus for Type-III Seesaw scenario β_{λ_h} becomes unstable $\sim 10^{10.7}$ GeV but bounce back to stability (where $\lambda_h \geq 0$) at $\sim 10^{14}$ GeV. For ID+ Type-III scenario, β_{λ_h} remains stable till Planck scale for $\lambda_i = 0.01$ and $Y_N = 0.06$ respectively.

Figure 5 (b) describes the behaviour two generations of fermionic triplet with reduced positive g_2 effect, which prohibits the Landau pole of λ_1 . We can see the ID+Type-III+ISS (purple curve) is more stable than Type-III+ISS (green curve). Again without ISS, the g_2 contribution is less so Type-III (red) and ID+Type-III (blue) have gone more negative; especially Type-III (red) is even more negative due to the lack of positive effects of ID scalars.

In Figure 6 we describe the behaviour of two-loop running of the SM-like Higgs quartic coupling λ_h as a function of scale (μ) for six benchmark points. We follow the same colour code as Figure 5 and $\lambda_1(EW) = 0.1264$ chosen for all the graphs. Figure 6(a) describes for the benchmark points of $\lambda_i = 0.01$, $Y_N = 0.01$ and $M_N = 100$ GeV where $i = 2, 3, 4, 5$ with two generations of Type-III fermions. We can clearly see that the stability scales for ID+Type-III+ISS (purple curve) and Type-III+ISS (green) are enhanced to Planck scale. Type-III (red) and ID+Type-III (blue) hit instability around $10^{9.5}$ GeV. Now if we increase $Y_N = 0.23$ as shown in Figure 6(b), we can see that red and blue curve hit instability earlier around $10^{8.5}$ GeV due to larger negative effects of Y_N . Even green and purple curves also hit $\lambda_h = 0$ due to this negative effect. For a comparative study with Figure 6(a) we plot the running of the λ_h for three generations of Type-III fermions in Figure 6(c). We see that the purple and the green curve hits Landau pole again due to larger positive g_2 contributions as explained earlier. Blue and red curve also move towards stability in this case. Figure 6(e) we restrict the fermion generation only to two and with the reduced positive effect the Landau poles are gone with overall shift towards the left.

Figure 6(d) shows the comparison with Figure 6(b) with two Type-III fermion generation with Y_N enhanced to 0.334. We notice the overall negative effect that shifts all the curves towards the left reducing the instability scale with red curve hitting instability at first at 10^7 GeV. If we increase the number of fermion generation to three in Figure 6(f) the effect will be enhanced as red curve crosses zero at around 10^6 GeV before acquiring the Landau pole at 10^{15} GeV. The shapes of all the curves becomes more steeper as compared to Figure 6(d). Compared to Figure 6(c) where $Y_N = 0.02$, if we increase $Y_N = 0.334$ in Figure 6(f), we see that the negative effect creeps in and the Type-III + ISS i.e. green the green curve does not hit the Landau pole. However, in ID+Type-III +ISS case due to the positive contributions from λ_i the purple curve hits the Landau pole at 10^{15} GeV.

4.2 Variation perturbativity and stability with Y_N

The variation of the stability scale with the size of Y_N and λ_i is depicted in Figure 7. For smaller values of λ_i , say 0.1 (green circles), the stability can be ensured up to the Planck scale only for $Y_N \leq 0.32$. In this case λ_1 strikes the perturbative bounds before other quartic couplings due to the strong g_2 effect and as $\lambda_1(EW) = 0.1264$. The other quartic coupling effects are negligible in this region as explained earlier.

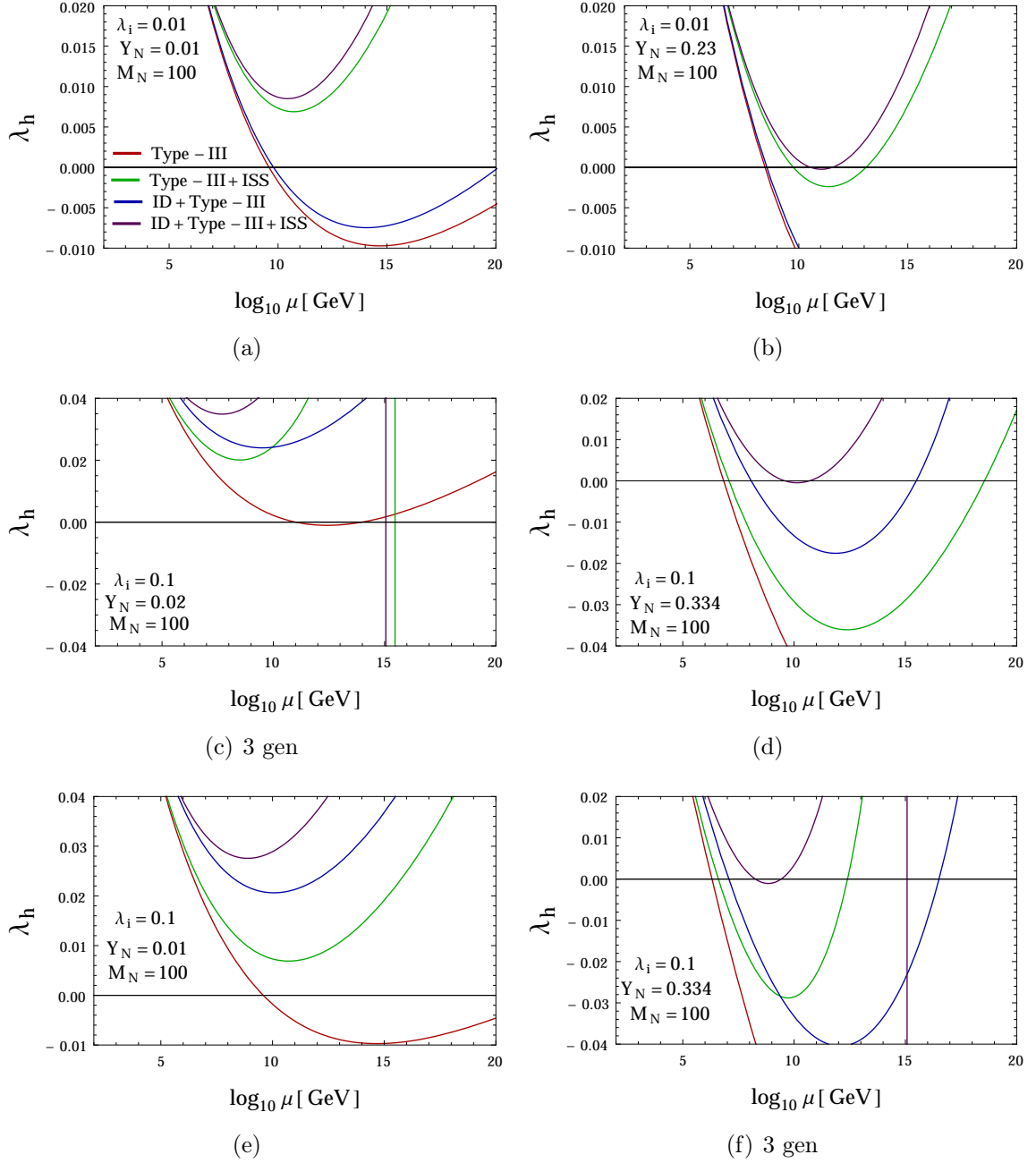


Figure 6. Two-loop running of the SM-like Higgs quartic coupling λ_h as a function of scale (μ). Here the red, green, blue and the purple curve corresponds to the Type-III, Type-III+ISS, ID+Type-III and ID+Type-III +ISS scenarios respectively for four different benchmark values of Y_N and Higgs quartic couplings ($\lambda_{1=2,3,4,5}$) with two generations of fermionic triplet. (c) and (f) are with three-generations of triplet fermions.

After $Y_N \geq 0.32$ (green line) the negative contribution from the new fermions take over and pull λ_h to negative values at around 10^9 GeV.

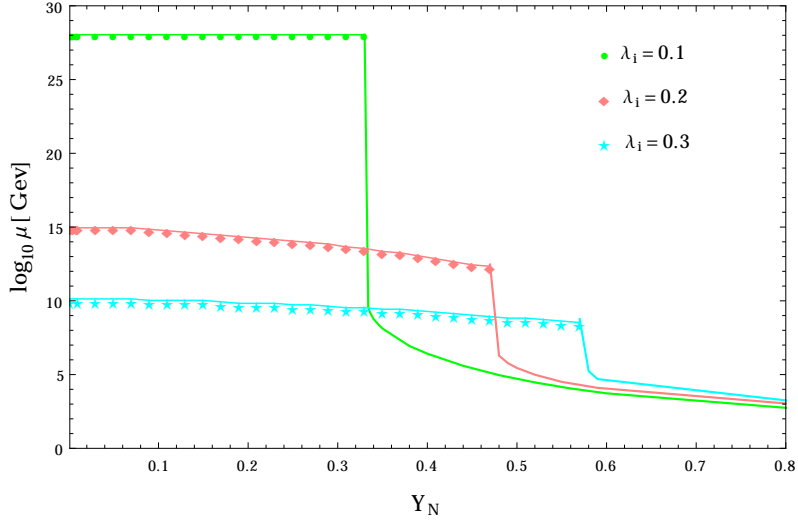


Figure 7. Effect of Yukawa coupling on the perturbativity and stability bound for different values of λ_i . Here, the green curve corresponds to $\lambda_i = 0.10$ which gives perturbativity and stability till the Planck scale for $Y_N \leq 0.32$. The pink curve corresponds to $\lambda_i = 0.2$ which gives Landau pole for $Y_N \leq 0.47$ (shown by diamond). After $Y_N = 0.47$, the negative fermionic contribution starts dominating which makes the $\lambda_h \leq 0$ for $10^{6.24}$ GeV (shown by pink line) before hitting the Landau pole. For $\lambda_i = 0.3$, the running of β_{λ_1} hits the Landau pole till $Y_N \leq 0.57$ (described by cyan color star) and later the effect of fermions makes the $\lambda_h \leq 0$ for $10^{5.23}$ GeV (described by cyan line).

For example as we enhance the λ_i at EW scale the effect of quartic couplings in their beta functions increase as $\lambda_i \text{Tr}(Y_N^\dagger Y_N)$ along with the enhanced g_2 effect. These inflate β_{λ_1} towards the higher scale stability compared the SM but leads to non-perturbative limit for the other λ_i s at lower scale. The point to be noted here is that for the choices of $\lambda_i > \lambda_1$ at the EW scale, other λ_i ($i = 2, 3, 4, 5$) are most likely to hit the Landau pole before λ_1 . For example as we enhance the $\lambda_i = 0.2$ with $\lambda_1 = 0.1264$ at the EW scale, one of the λ_i s afflicts the landau pole (shown by pink color diamond) around $10^{15} - 10^{12}$ GeV, even before λ_1 enters into instability at $Y_N = 0.47$ for $10^{6.24}$ GeV (shown by pink line). The bending of the curves for higher Y_N are due to the positive $\lambda_i \text{Tr}(Y_N^\dagger Y_N)$ effect for perturbativity and negative $\text{Tr}(Y_N^\dagger Y_N Y_N^\dagger Y_N)$ effect for the instability respectively.

For $\lambda_i = 0.3$, one of the λ_i s hits the Landau pole at much lower scale around 10^{10} GeV (cyan colour star) due to large quartic coupling contributions along with $\lambda_i \text{Tr}(Y_N^\dagger Y_N)$. In this case the negative effect of Y_N in λ_1 starts much later due to larger value of λ_i and at $Y_N \geq 0.57$ the effect of fermions make the $\lambda_h \leq 0$ for $10^{5.23}$ GeV (cyan line).

4.3 Vacuum Stability from RG-improved potential Approach

In this section, we investigate the stability of the EW vacuum at one-loop level. Here we follow the Coleman and Weinberg [84] prescription of RG-improved effective potential and calculate the effective potential at one-loop for the scenario of SM + Type-III-ISS + ID with two generations of fermions. The parameter space of the model is scanned for the stability, metastability and instability of the potential by calculating the effective Higgs quartic coupling, and putting appropriate limits which constrain the model parameter space.

The tree-level Higgs potential of our model is given in Eq. (2.3). The conditions that satisfy that the potential is bounded from below in all the directions at the tree-level are given by [71]

$$\lambda_1 \geq 0, \quad \lambda_2 \geq 0, \quad \lambda_3 \geq -\sqrt{\lambda_1 \lambda_2}, \quad \lambda_3 + \lambda_4 - |\lambda_5| \geq -\sqrt{\lambda_1 \lambda_2}. \quad (4.5)$$

We know that the Higgs quartic coupling λ_h gets a negative contribution from top Yukawa coupling y_t , which makes it negative around 10^{10-11} GeV in SM and we expect a second deeper minimum for the high field values via quantum corrections. Since the second minimum exists at much higher scale than the EW minimum, we can safely consider the effective potential in the h -direction to be

$$V_{\text{eff}}(h, \mu) \simeq \lambda_{\text{eff}}(h, \mu) \frac{h^4}{4}, \quad \text{with } h \gg v, \quad (4.6)$$

where $\lambda_{\text{eff}}(h, \mu)$ is the effective quartic coupling which can be calculated from the RG-improved potential. Then the stability of the vacuum then be guaranteed at a given scale μ by demanding that $\lambda_{\text{eff}}(h, \mu) \geq 0$. We follow the same strategy as in the SM in order to calculate $\lambda_{\text{eff}}(h, \mu)$ in our model, as described below.

4.4 Effective Potential

The one-loop RG-improved effective potential in our model can be written as

$$V_{\text{eff}} = V_0 + V_1^{\text{SM}} + V_1^{\text{ID}} + V_1^{\text{ISS+Type-III}}, \quad (4.7)$$

where V_0 is the tree-level potential given by Eq. (2.3), V_1^{SM} is the effective Coleman-Weinberg potential in the SM that contains all the one-loop corrections involving the SM particles at zero temperature with vanishing momenta. The other two terms V_1^{ID} and $V_1^{\text{ISS+Type-III seesaw}}$ represent the corresponding one-loop effective potential terms from the inert scalar doublet, and fermionic triplet, respectively. In general, V_1 can be written as

$$V_1(h, \mu) = \frac{1}{64\pi^2} \sum_i (-1)^F n_i M_i^4(h) \left[\log \frac{M_i^2(h)}{\mu^2} - c_i \right], \quad (4.8)$$

where the sum runs over all the particles that couple to the h -field, $F = 0$ for bosons in the loop and 1 for the fermions, n_i is the number of degrees of freedom of each particle and M_i^2 are the tree-level field-dependent masses given by

$$M_i^2(h) = \kappa_i h^2 - \kappa'_i, \quad (4.9)$$

with the coefficients given in Table 1. In the last column, m^2 corresponds to the Higgs mass parameter at tree-level. Note that the particles which are massless do not contribute to Eq. (4.9), and hence, neither to Eq. (4.8). Therefore, for the SM fermions, we only include the dominant contribution from top quarks, and neglect the other quarks contribution. It is also important to note that the ISS contributions come after each threshold value of M_{N_i} . Using Eq. (4.8) for the one-loop potentials,

Particles	i	F	n_i	c_i	κ_i	κ'_i
SM	W^\pm	0	6	5/6	$g_2^2/4$	0
	Z	0	3	5/6	$(g_1^2 + g_2^2)/4$	0
	t	1	12	3/2	Y_t^2	0
	h	0	1	3/2	λ_h	m^2
	G^\pm	0	2	3/2	λ_h	m^2
	G^0	0	1	3/2	λ_h	m^2
Inert	H^\pm	0	2	3/2	$\lambda_3/2$	0
	H	0	1	3/2	$(\lambda_3 + \lambda_4 + 2\lambda_5)/2$	0
	A	0	1	3/2	$(\lambda_3 + \lambda_4 - 2\lambda_5)/2$	0
Type3seesaw +ISS	Σ_{1i}	1	2	3/2	$Y_N^2/2$	0

Table 1. Coefficients entering in the Coleman-Weinberg effective potential, cf. Eq. (4.8).

the full effective potential in Eq. (4.7) can be written in terms of an effective quartic coupling as in Eq. (4.6). This effective coupling can be written as follows:

$$\begin{aligned}
\lambda_{\text{eff}}(h, \mu) \simeq & \underbrace{\lambda_h(\mu)}_{\text{tree-level}} + \frac{1}{16\pi^2} \left\{ \underbrace{\sum_{i=W^\pm, Z, t, h, G^\pm, G^0} n_i \kappa_i^2 \left[\log \frac{\kappa_i h^2}{\mu^2} - c_i \right]}_{\text{Contribution from SM}} + \underbrace{\sum_{i=H, A, H^\pm} n_i \kappa_i^2 \left[\log \frac{\kappa_i h^2}{\mu^2} - c_i \right]}_{\text{Contribution from ID}} \right. \\
& \left. + 2 \underbrace{\sum_{i=1,2} n_i \kappa_i^2 \left[\log \frac{\kappa_i h^2}{\mu^2} - c_i \right]}_{\text{Contribution from Type-III+ISS}} \right\}. \quad (4.10)
\end{aligned}$$

Note that in the inverse seesaw case and in the limit $\mu_\Sigma \rightarrow 0$, each of the triplet fermion mass eigenvalue is double-degenerate, and therefore, we have an extra factor of two for each new Type-III fermion contribution in Eq. (4.10). The nature of

$\lambda_{\text{eff}}(h, \mu)$ in our model thus guides us to identify the possible stability, metastability and instability regions. We take the field value $h = \mu$ for the numerical analysis as at that scale the potential remains scale-invariant [85].

4.5 Stable, Metastable and Unstable Regions

The parameter space where $\lambda_{\text{eff}} \geq 0$ is termed as the *stable* region, since in this region the EW vacuum is the global minimum. For $\lambda_{\text{eff}} < 0$, there exists a second minimum deeper than the EW vacuum. In this case, the EW vacuum could be either metastable or unstable, depending on the tunnelling probability from the EW vacuum to the true vacuum. The parameter space with $\lambda_{\text{eff}} < 0$, but with the tunnelling lifetime longer than the age of the universe is termed as the *metastable* region. The expression for the tunnelling probability from the EW vacuum to the deeper vacuum at zero temperature is given by

$$P = T_0^4 \mu^4 \exp \left[\frac{-8\pi^2}{3\lambda_{\text{eff}}(\mu)} \right], \quad (4.11)$$

where T_0 is the age of the universe, and μ denotes the scale where the probability is maximized, i.e. $\frac{\partial P}{\partial \mu} = 0$. This gives us a relation between the λ values at different scales:

$$\lambda_{\text{eff}}(\mu) = \frac{\lambda_{\text{eff}}(v)}{1 - \frac{3}{2\pi^2} \log \left(\frac{v}{\mu} \right) \lambda_{\text{eff}}(v)}, \quad (4.12)$$

where $v \simeq 246$ GeV is the EW VEV. Setting $P = 1$, $T = 10^{10}$ years and $\mu = v$ in Eq. (4.11), we find $\lambda_{\text{eff}}(v) = 0.0623$. The condition $P < 1$, for a universe about $T = 10^{10}$ years old is equivalent to the requirement that the tunneling lifetime from the EW vacuum to the deeper one is larger than T_0 and we obtain the metastability condition as follows [6]:

$$0 > \lambda_{\text{eff}}(\mu) \gtrsim \frac{-0.065}{1 - 0.01 \log \left(\frac{v}{\mu} \right)}. \quad (4.13)$$

The remaining parameter space with $\lambda_{\text{eff}} < 0$, where the above mentioned condition (4.13) is not satisfied is termed as the *unstable* region. As can be seen from Eq. (4.10), these regions depend on the energy scale μ , as well as the model parameters, including the triplet fermion mass and the gauge, scalar quartic and Yukawa couplings.

Figure 8 represents the phase diagrams in terms of Higgs boson mass and top quark pole mass in GeV. The red, yellow and green regions correspond to the unstable, metastable and stable regions, respectively. The contours and the dot show the current experimental $1\sigma, 2\sigma, 3\sigma$ regions and the central value in the (M_h, M_t) plane [9, 27]. To obtain the regions we vary all the $\lambda_i = 0.1 - 0.8$ while the λ_1 and y_t

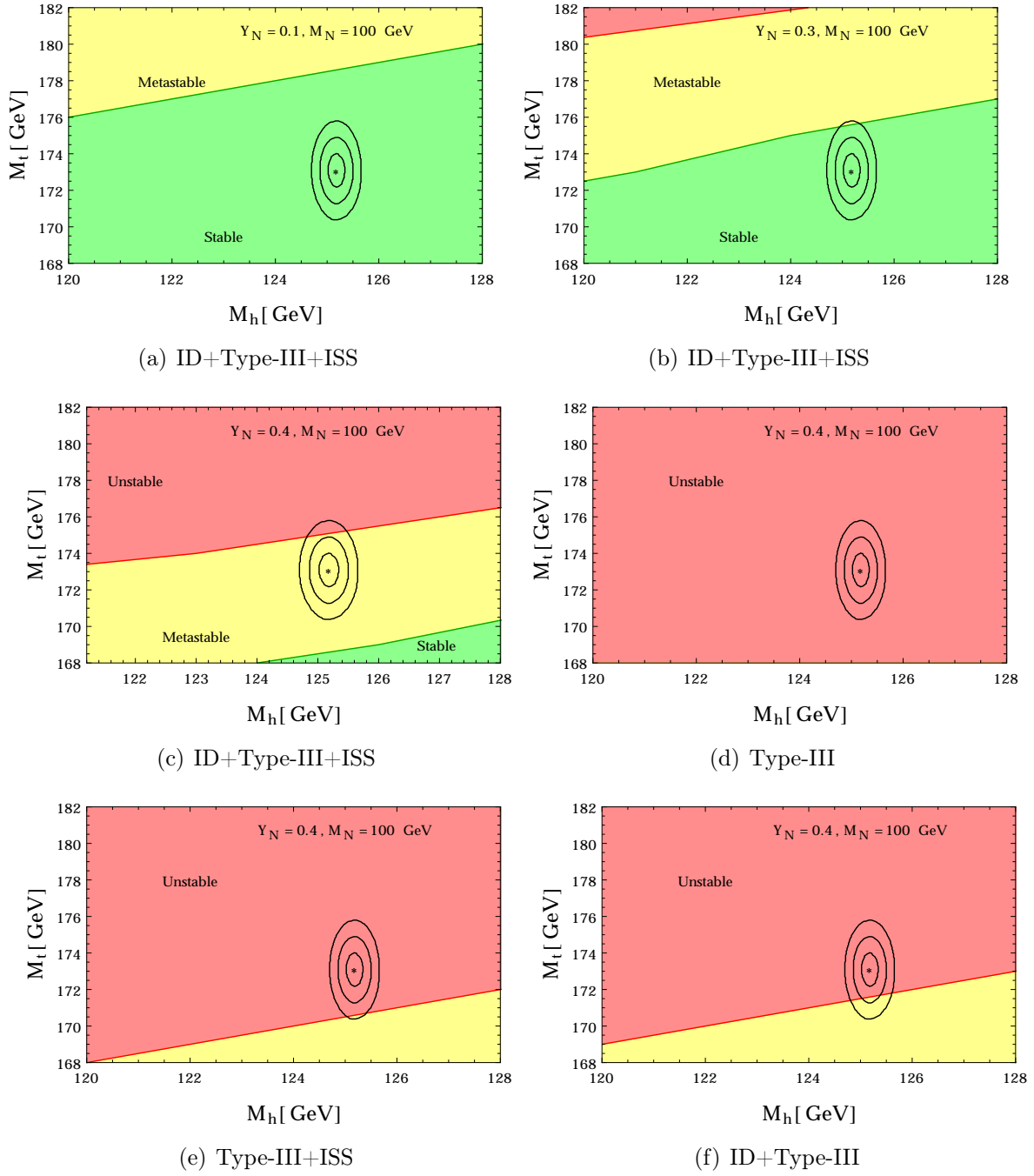


Figure 8. Phase diagram in terms of Higgs and top pole masses in GeV with $M_N = 100$ GeV in Figure 8(a), 8(b), 8(c) for ID+Type-III+ISS scenarios with $Y_N = 0.1, 0.3, 0.4$ respectively. Figure 8(d) is for Type-III only and Figure 8(e), 8(f) are for Type-III+ISS with $Y_N = 0.4$. The red, yellow and green regions correspond to the unstable, metastable and stable regions, respectively. The contours and the dot show the current experimental $1\sigma, 2\sigma, 3\sigma$ regions and central value in the (M_h, M_t) plane.

are varied to attained the Higgs boson mass within $120 - 128$ GeV and top quark mass within $168 - 182$ GeV respectively. In Figure 8 we fix $M_N = 100$ GeV and vary $Y_N = 0.1 - 0.4$ for two generations of $SU(2)$ triplet fermions. Figure 8(a) and Figure 8(b) present the scenarios with ID+Type-III+ISS for relatively lower values of $Y_N = 0.1, 0.3$. It is realized that the scenarios are stable till Planck scale.

As shown in Figure 8(a), in this scenario, λ_{eff} becomes more positive and the region is fully in the stable region till Planck scale. This occurs, as there is more positive contribution from g_2 compared to negative effect from fermions for lower values of Y_N . Additionally, the inert doublet also adds more scalars to the effective potential, leading to the enhanced stability. In Figure 8(b) we depict the scenario for $Y_N = 0.3$, where negative fermionic effect starts showing up which is compensated by the scalar effect of IDM. As is evident, the stability is still more than SM, and hence, the 3σ contour in $m_h - m_t$ plane just touches the region of metastability. Further enhancement in the value of Y_N counters the positive scalar effect of IDM, and for $Y_N = 0.4$ the 2σ region enters in the unstable region as described in Figure 8(c).

Figure 8(d) describes the scenario for Type-III seesaw with two generations triplet fermions, assuming $Y_N = 0.4$. It can be seen that the whole region is unstable. Further addition of ISS $SU(2)_L$ triplet fermions which directly do not give negative contributions but enhance g_2 to more positive value as discussed before leads to Type-III seesaw+ISS scenario marginally extending into the metastable region for $Y_N = 0.4$, as depicted in Figure 8(e). Instead of ISS fermions addition of inert doublet also have the similar effect and pushes the potential into the metastable region as shown in Figure 8(f). This further motivates the extension of Type-III seesaw scenario with ISS and IDM to achieve the stability at larger values of Y_N as described in Figure 8(d).

Figure 9 we increase $M_N = 10^3$ GeV and analyse the phase diagrams as before. Due to this enhancement in $SU(2)_L$ triplet fermion mass their negative loop effects will now be reduced. This can be realised from Figure 9(a)-9(b), where λ_{eff} is highly positive and the regions are fully stable as compared to Figure 8(a)-8(b). As we increase $Y_N = 0.4$, the negative fermionic effect starts showing up in Figure 9(c). The region now lies in the metastable region, however touching the stable region, contrary to Figure 8(c) where some part is in unstable region.

Figure 9(d) describes the only Type-III scenario for $Y_N = 0.4$ in which the central value in the (M_h, M_t) plane lies in the unstable region similar to Figure 8(d). An extension of Type-III seesaw with ISS in Figure-9(e) and an extension of Type-III seesaw with inert doublet in Figure 9(f) moves the potential into the metastable region similar to $M_N = 100$ GeV case in Figure 8(e)-8(f) respectively.

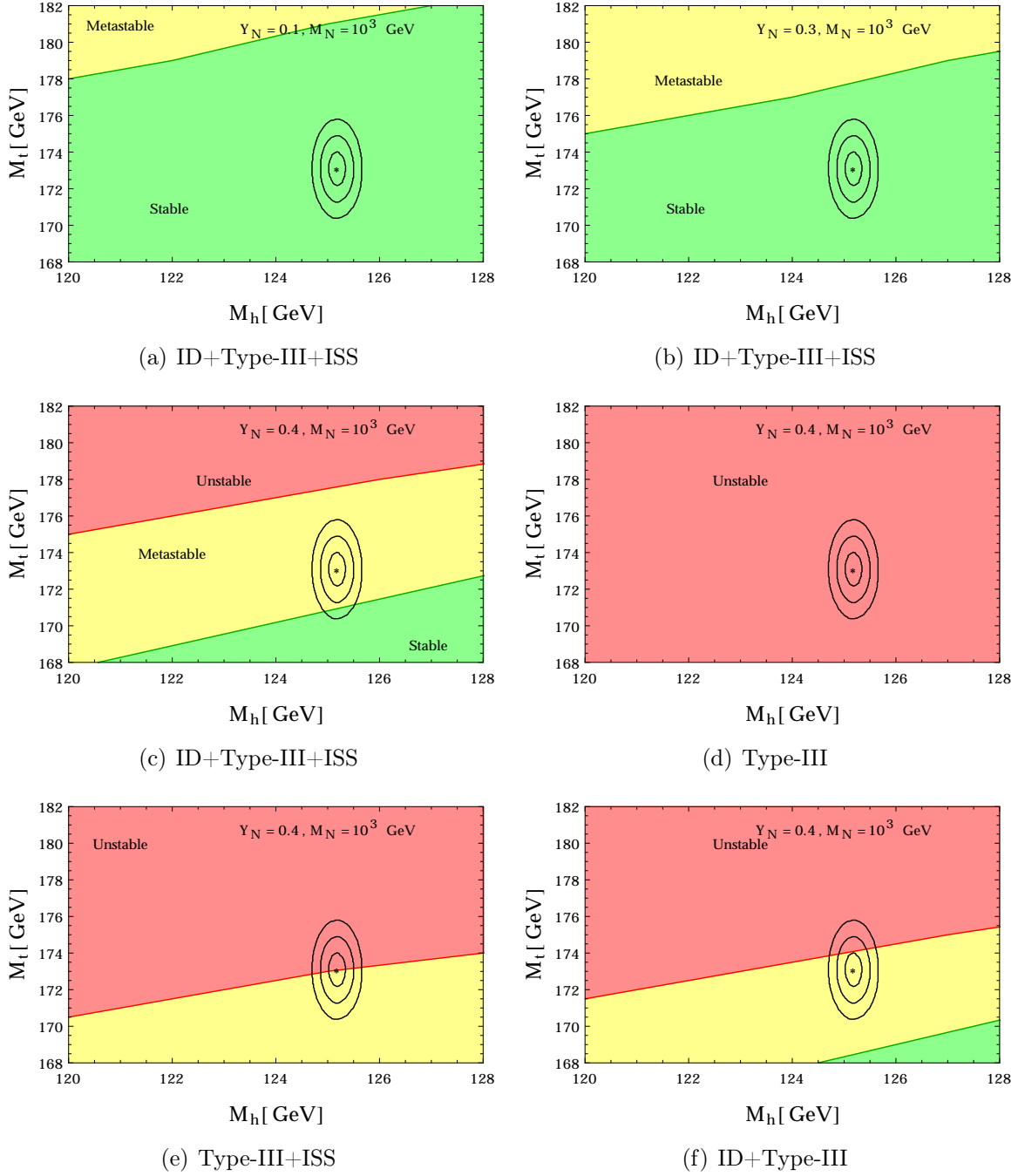


Figure 9. Phase diagram in terms of Higgs and top pole masses in GeV with $M_N = 10^3$ GeV in Figure 9(a), 9(b), 9(c) for ID+Type-III+ISS scenarios with $Y_N = 0.1, 0.3, 0.4$ respectively. Figure 9(d) is for Type-III only and Figure 9(e), 9(f) are for Type-III+ISS with $Y_N = 0.4$. The red, yellow and green regions correspond to the unstable, metastable and stable regions, respectively. The contours and the dot show the current experimental $1\sigma, 2\sigma, 3\sigma$ regions and central value in the (M_h, M_t) plane.

5 Discussions and conclusion

In this article we studied the vacuum stability of the electroweak vacuum in the presence of Type-III fermions along with inverse seesaw fermions. Unlike Type-I seesaw case, Type-III fermions are in the triplet representation of $SU(2)$ which contribute to the beta-function of the gauge coupling g_2 even at one-loop level. This is a positive effect and increases from Type-III to Type-III+ISS+ID case step wise and makes the g_2 grow to higher values as scale increases. g_2 certainly becomes not perturbative below Planck scale or GUT scale for three generations of Type-III fermions. It is only with the two generation that we are able to acquire the Planck or GUT scale stability.

The enhancement of g_2 also has impact on the scalar quartic couplings which makes them non-perturbative much before compared to SM or SM+Type-I+ISS [19]. For lower values of quartic couplings the g_2 effect is the dominant. At larger values of λ_i (except the λ_1 which is fixed by the Higgs mass at EW scale) $\lambda_i \text{Tr}(Y_N^\dagger Y_N)$ effect creeps in making the quartic couplings further divergent. However, a further increment of Y_N will bring down the stability bound by pushing λ_1 to negative direction which is proportional to $\text{Tr}(Y_N^\dagger Y_N Y_N^\dagger Y_N)$. For Planck scale perturbativity we can go up to $\lambda_5 \sim 0.17$ with $\lambda_1 = 0.126$ and other $\lambda_i = 0.10$ at the EW scale for $Y_N = 0.40$. The effective potential approach calculations show that even for $Y_N = 0.30$ for $m_N = 100, 1000$ GeV the model ID+Type-III+ISS with two generations of new fermions lies in the stable region for lower values of Y_N and draws to metastable region for higher values of Y_N . However, only Type-III scenario belongs to unstable regions in both cases, whereas ID+Type-III and Type-III+ISS scenarios can be in between metastable and unstable regions.

IDM is generally motivated to provide the much needed DM to explain the DM relic and other experimental observations. Nevertheless, it is also supported to enhance the stability of electroweak vacuum. Being in Z -odd multiplet it does not couple to the $SU(2)$ triplet fermions which makes their phenomenology more illusive. No two-body decays are allowed for the Type-III fermions into any of the inert Higgs bosons. In [16, 19] authors have shown that due to compressed spectrum only some three- and four-body decays are allowed maintaining the Z_2 symmetry of the Lagrangian. In [15, 16, 86–88] a detailed relic calculations has been carried out including the direct, indirect DM searches and collider phenomenology. It has been found out that the lightest Z_2 -odd particles should be heavier than 1176 GeV to satisfy the DM relic constraints which is in the desired range to explain the AMS-02 positron excess observation [16, 89]. The decays of charged Higgs boson can give rise to mono-lepton plus missing energy signatures [16] which can isolated from displaced mono-leptonic signatures in real scalar and complex triplet scenarios [16, 90] and other charged Higgs signatures [81, 91–93]. Similar displaced charged leptonic signatures can be observed in the models with Type-I seesaw [81, 94–97]

and Type-III seesaw[45, 98, 99].

The triplet fermions are searched at the LHC at 13 TeV centre of mass energy with democratic branching fractions [100] and a lower bound of 620 – 840 GeV has been put at 2σ level. However, due the presence and mixing with other set of $SU(2)$ triplet fermions involving in inverse seesaw and non-democratic branching can substantially reduce the mass limit allowing even smaller triplet fermion mass. Type-III fermions can also be looked via their angular distributions at the LHC [54].

Acknowledgments

SJ thanks DST/INSPIRES/03/2018/001207 for the financial support towards the PhD program. SJ also wants to thank Dr. Anirban Karan for useful discussions. PB wants to thank SERB CORE Grant CRG/2018/004971 and Anomalies 2019-IUSSTF for the support. PB thanks Prof. Debajyoti Chaudhury for useful discussion. PB and SJ also want to thank Mr. Saiyad Ashanujjaman for the help in SARAH. PB and SJ also thank IOPB for the visit and local hospitality in the early part of the project.

A Two-loop β -functions-With two generations

A.1 Scalar Quartic Couplings

$$\begin{aligned}
\beta_{\lambda_1} = & \frac{1}{16\pi^2} \left[\frac{27}{200}g_1^4 + \frac{9}{20}g_1^2g_2^2 + \frac{9}{8}g_2^4 - \frac{9}{5}g_1^2\lambda_1 - 9g_2^2\lambda_1 + 24\lambda_1^2 + 2\lambda_3^2 + 2\lambda_3\lambda_4 + \lambda_4^2 + 4\lambda_5^2 \right. \\
& + 12\lambda_1\text{Tr}(Y_dY_d^\dagger) + 4\lambda_1\text{Tr}(Y_eY_e^\dagger) + 12\lambda_1\text{Tr}(Y_NY_N^\dagger) + 12\lambda_1\text{Tr}(Y_uY_u^\dagger) - 6\text{Tr}(Y_dY_d^\dagger Y_dY_d^\dagger) \\
& - 2\text{Tr}(Y_eY_e^\dagger Y_eY_e^\dagger) - 8\text{Tr}(Y_eY_N^\dagger Y_NY_e^\dagger) - 10\text{Tr}(Y_NY_N^\dagger Y_NY_N^\dagger) - 6\text{Tr}(Y_uY_u^\dagger Y_uY_u^\dagger) \Big] \\
& + \frac{1}{(16\pi^2)^2} \left[-\frac{3537}{2000}g_1^6 - \frac{1719}{400}g_1^4g_2^2 - \frac{559}{80}g_1^2g_2^4 + \frac{35}{16}g_2^6 + \frac{1953}{200}g_1^4\lambda_1 + \frac{117}{20}g_1^2g_2^2\lambda_1 + \frac{269}{8}g_2^4\lambda_1 \right. \\
& + 108g_2^2\lambda_1^2 - 312\lambda_1^3 + \frac{9}{10}g_1^4\lambda_3 + \frac{15}{2}g_2^4\lambda_3 + \frac{12}{5}g_1^2\lambda_3^2 + 12g_2^2\lambda_3^2 - 20\lambda_1\lambda_3^2 - 8\lambda_3^3 + \frac{9}{20}g_1^4\lambda_4 \\
& + \frac{3}{2}g_1^2g_2^2\lambda_4 + \frac{15}{4}g_2^4\lambda_4 + \frac{12}{5}g_1^2\lambda_3\lambda_4 + 12g_2^2\lambda_3\lambda_4 - 20\lambda_1\lambda_3\lambda_4 - 12\lambda_3^2\lambda_4 + \frac{6}{5}g_1^2\lambda_4^2 \\
& + 3g_2^2\lambda_4^2 - 12\lambda_1\lambda_4^2 - 16\lambda_3\lambda_4^2 - 6\lambda_4^3 - \frac{12}{5}g_1^2\lambda_5^2 - 56\lambda_1\lambda_5^2 - 80\lambda_3\lambda_5^2 - 88\lambda_4\lambda_5^2 + \frac{108}{5}g_1^2\lambda_1^2 \\
& + \frac{1}{20} \left(-5(64\lambda_1(-5g_3^2 + 9\lambda_1) - 90g_2^2\lambda_1 + 9g_2^4) + 9g_1^4 + g_1^2(50\lambda_1 + 54g_2^2) \right) \text{Tr}(Y_dY_d^\dagger) \\
& - \frac{3}{20} \left(15g_1^4 - 2g_1^2(11g_2^2 + 25\lambda_1) + 5(-10g_2^2\lambda_1 + 64\lambda_1^2 + g_2^4) \right) \text{Tr}(Y_eY_e^\dagger) - \frac{27}{100}g_1^4\text{Tr}(Y_NY_N^\dagger) \\
& - \frac{57}{10}g_1^2g_2^2\text{Tr}(Y_NY_N^\dagger) + \frac{7}{4}g_2^4\text{Tr}(Y_NY_N^\dagger) + \frac{9}{2}g_1^2\lambda_1\text{Tr}(Y_NY_N^\dagger) + \frac{165}{2}g_2^2\lambda_1\text{Tr}(Y_NY_N^\dagger) \\
& - 144\lambda_1^2\text{Tr}(Y_NY_N^\dagger) - \frac{171}{100}g_1^4\text{Tr}(Y_uY_u^\dagger) + \frac{63}{10}g_1^2g_2^2\text{Tr}(Y_uY_u^\dagger) - \frac{9}{4}g_2^4\text{Tr}(Y_uY_u^\dagger) \Big]
\end{aligned}$$

$$\begin{aligned}
& + \frac{17}{2}g_1^2\lambda_1\text{Tr}(Y_uY_u^\dagger) + \frac{45}{2}g_2^2\lambda_1\text{Tr}(Y_uY_u^\dagger) + 80g_3^2\lambda_1\text{Tr}(Y_uY_u^\dagger) - 144\lambda_1^2\text{Tr}(Y_uY_u^\dagger) \\
& + \frac{4}{5}g_1^2\text{Tr}(Y_dY_d^\dagger Y_dY_d^\dagger) - 32g_3^2\text{Tr}(Y_dY_d^\dagger Y_dY_d^\dagger) - 3\lambda_1\text{Tr}(Y_dY_d^\dagger Y_dY_d^\dagger) - 42\lambda_1\text{Tr}(Y_dY_u^\dagger Y_uY_d^\dagger) \\
& - \frac{12}{5}g_1^2\text{Tr}(Y_eY_e^\dagger Y_eY_e^\dagger) - \lambda_1\text{Tr}(Y_eY_e^\dagger Y_eY_e^\dagger) - \frac{24}{5}g_1^2\text{Tr}(Y_eY_N^\dagger Y_NY_e^\dagger) + 30\text{Tr}(Y_uY_u^\dagger Y_uY_u^\dagger Y_uY_u^\dagger) \\
& - 16g_2^2\text{Tr}(Y_eY_N^\dagger Y_NY_e^\dagger) + 38\lambda_1\text{Tr}(Y_eY_N^\dagger Y_NY_e^\dagger) - 40g_2^2\text{Tr}(Y_NY_N^\dagger Y_NY_N^\dagger) \\
& - 5\lambda_1\text{Tr}(Y_NY_N^\dagger Y_NY_N^\dagger) - \frac{8}{5}g_1^2\text{Tr}(Y_uY_u^\dagger Y_uY_u^\dagger) - 32g_3^2\text{Tr}(Y_uY_u^\dagger Y_uY_u^\dagger) - 3\lambda_1\text{Tr}(Y_uY_u^\dagger Y_uY_u^\dagger) \\
& + 30\text{Tr}(Y_dY_d^\dagger Y_dY_d^\dagger Y_dY_d^\dagger) - 12\text{Tr}(Y_dY_d^\dagger Y_dY_u^\dagger Y_uY_d^\dagger) + 6\text{Tr}(Y_dY_u^\dagger Y_uY_d^\dagger Y_dY_d^\dagger) \\
& - 6\text{Tr}(Y_dY_u^\dagger Y_uY_u^\dagger Y_uY_d^\dagger) + 10\text{Tr}(Y_eY_e^\dagger Y_eY_e^\dagger Y_eY_e^\dagger) + 36\text{Tr}(Y_eY_e^\dagger Y_eY_N^\dagger Y_NY_e^\dagger) \\
& + 38\text{Tr}(Y_eY_N^\dagger Y_NY_e^\dagger Y_eY_e^\dagger) + 150\text{Tr}(Y_eY_N^\dagger Y_NY_N^\dagger Y_NY_e^\dagger) + 94\text{Tr}(Y_NY_N^\dagger Y_NY_N^\dagger Y_NY_N^\dagger) \Big] . \\
\beta_{\lambda_2} = & \frac{1}{16\pi^2} \left[24\lambda_2^2 + 2\lambda_3^2 + 2\lambda_3\lambda_4 + 4\lambda_5^2 - 9g_2^2\lambda_2 + \frac{27}{200}g_1^4 + \frac{9}{20}g_1^2(-4\lambda_2 + g_2^2) + \frac{9}{8}g_2^4 + \lambda_4^2 \right] \\
& + \frac{1}{(16\pi^2)^2} \left[-\frac{3537}{2000}g_1^6 - \frac{1719}{400}g_1^4g_2^2 - \frac{559}{80}g_1^2g_2^4 + \frac{35}{16}g_2^6 + \frac{1953}{200}g_1^4\lambda_2 + \frac{117}{20}g_1^2g_2^2\lambda_2 + \frac{269}{8}g_2^4\lambda_2 \right. \\
& + 108g_2^2\lambda_2^2 - 312\lambda_3^2 + \frac{9}{10}g_1^4\lambda_3 + \frac{15}{2}g_2^4\lambda_3 + \frac{12}{5}g_1^2\lambda_3^2 + 12g_2^2\lambda_3^2 - 20\lambda_2\lambda_3^2 - 8\lambda_3^3 + \frac{9}{20}g_1^4\lambda_4 \\
& + \frac{3}{2}g_1^2g_2^2\lambda_4 + \frac{15}{4}g_2^4\lambda_4 + \frac{12}{5}g_1^2\lambda_3\lambda_4 + 12g_2^2\lambda_3\lambda_4 - 20\lambda_2\lambda_3\lambda_4 - 12\lambda_3^2\lambda_4 + \frac{6}{5}g_1^2\lambda_4^2 + \frac{108}{5}g_1^2\lambda_2^2 \\
& + 3g_2^2\lambda_4^2 - 12\lambda_2\lambda_4^2 - 16\lambda_3\lambda_4^2 - 6\lambda_4^3 - \frac{12}{5}g_1^2\lambda_5^2 - 56\lambda_2\lambda_5^2 - 80\lambda_3\lambda_5^2 - 88\lambda_4\lambda_5^2 \\
& - 6(2\lambda_3^2 + 2\lambda_3\lambda_4 + 4\lambda_5^2 + \lambda_4^2)\text{Tr}(Y_dY_d^\dagger) - 2(2\lambda_3^2 + 2\lambda_3\lambda_4 + 4\lambda_5^2 + \lambda_4^2)\text{Tr}(Y_eY_e^\dagger) \\
& - 12\lambda_3^2\text{Tr}(Y_NY_N^\dagger) - 12\lambda_3\lambda_4\text{Tr}(Y_NY_N^\dagger) - 6\lambda_4^2\text{Tr}(Y_NY_N^\dagger) - 24\lambda_5^2\text{Tr}(Y_NY_N^\dagger) \\
& \left. - 12\lambda_3^2\text{Tr}(Y_uY_u^\dagger) - 12\lambda_3\lambda_4\text{Tr}(Y_uY_u^\dagger) - 6\lambda_4^2\text{Tr}(Y_uY_u^\dagger) - 24\lambda_5^2\text{Tr}(Y_uY_u^\dagger) \right] . \\
\beta_{\lambda_3} = & \frac{1}{16\pi^2} \left[\frac{27}{100}g_1^4 - \frac{9}{10}g_1^2g_2^2 + \frac{9}{4}g_2^4 - \frac{9}{5}g_1^2\lambda_3 - 9g_2^2\lambda_3 + 12\lambda_1\lambda_3 + 12\lambda_2\lambda_3 + 4\lambda_3^2 + 4\lambda_1\lambda_4 + 4\lambda_2\lambda_4 \right. \\
& \left. + 2\lambda_4^2 + 8\lambda_5^2 + 6\lambda_3\text{Tr}(Y_dY_d^\dagger) + 2\lambda_3\text{Tr}(Y_eY_e^\dagger) + 6\lambda_3\text{Tr}(Y_NY_N^\dagger) + 6\lambda_3\text{Tr}(Y_uY_u^\dagger) \right] \\
& + \frac{1}{(16\pi^2)^2} \left[-\frac{3537}{1000}g_1^6 + \frac{909}{200}g_1^4g_2^2 + \frac{289}{40}g_1^2g_2^4 + \frac{35}{8}g_2^6 + \frac{27}{10}g_1^4\lambda_1 - 3g_1^2g_2^2\lambda_1 + \frac{45}{2}g_2^4\lambda_1 + \frac{27}{10}g_1^4\lambda_2 \right. \\
& - 3g_1^2g_2^2\lambda_2 + \frac{45}{2}g_2^4\lambda_2 + \frac{1773}{200}g_1^4\lambda_3 + \frac{33}{20}g_1^2g_2^2\lambda_3 + \frac{209}{8}g_2^4\lambda_3 + \frac{72}{5}g_1^2\lambda_1\lambda_3 + 72g_2^2\lambda_1\lambda_3 \\
& - 60\lambda_1^2\lambda_3 + \frac{72}{5}g_1^2\lambda_2\lambda_3 + 72g_2^2\lambda_2\lambda_3 - 60\lambda_2^2\lambda_3 + \frac{6}{5}g_1^2\lambda_3^2 + 6g_2^2\lambda_3^2 - 72\lambda_1\lambda_3^2 - 72\lambda_2\lambda_3^2 \\
& - 12\lambda_3^3 + \frac{9}{10}g_1^4\lambda_4 - \frac{9}{5}g_1^2g_2^2\lambda_4 + \frac{15}{2}g_2^4\lambda_4 + \frac{24}{5}g_1^2\lambda_1\lambda_4 + 36g_2^2\lambda_1\lambda_4 - 16\lambda_1^2\lambda_4 + \frac{24}{5}g_1^2\lambda_2\lambda_4 \\
& + 36g_2^2\lambda_2\lambda_4 - 16\lambda_2^2\lambda_4 - 12g_2^2\lambda_3\lambda_4 - 32\lambda_1\lambda_3\lambda_4 - 32\lambda_2\lambda_3\lambda_4 - 4\lambda_3^2\lambda_4 - \frac{6}{5}g_1^2\lambda_4^2 \\
& \left. + 6g_2^2\lambda_4^2 - 28\lambda_1\lambda_4^2 - 28\lambda_2\lambda_4^2 - 16\lambda_3\lambda_4^2 - 12\lambda_4^3 + \frac{48}{5}g_1^2\lambda_5^2 - 144\lambda_1\lambda_5^2 - 144\lambda_2\lambda_5^2 \right]
\end{aligned}$$

$$\begin{aligned}
& -72\lambda_3\lambda_5^2 - 176\lambda_4\lambda_5^2 + \frac{1}{20} \left(-5 \left(-45g_2^2\lambda_3 + 8 \left(-20g_3^2\lambda_3 + 3 \left(2\lambda_3^2 + 4\lambda_1(3\lambda_3 + \lambda_4) \right. \right. \right. \right. \\
& \left. \left. \left. + 4\lambda_5^2 + \lambda_4^2 \right) \right) + 9g_2^4 \right) + 9g_1^4 + g_1^2(25\lambda_3 - 54g_2^2) \right) \text{Tr}(Y_d Y_d^\dagger) - \frac{1}{20} (45g_1^4 \\
& + 5 \left(-15g_2^2\lambda_3 + 3g_2^4 + 8 \left(2\lambda_3^2 + 4\lambda_1(3\lambda_3 + \lambda_4) + 4\lambda_5^2 + \lambda_4^2 \right) \right) + g_1^2(66g_2^2 - 75\lambda_3) \text{Tr}(Y_e Y_e^\dagger) \\
& - \frac{27}{100} g_1^4 \text{Tr}(Y_N Y_N^\dagger) + \frac{57}{10} g_1^2 g_2^2 \text{Tr}(Y_N Y_N^\dagger) + \frac{7}{4} g_2^4 \text{Tr}(Y_N Y_N^\dagger) + \frac{9}{4} g_1^2 \lambda_3 \text{Tr}(Y_N Y_N^\dagger) \\
& + \frac{165}{4} g_2^2 \lambda_3 \text{Tr}(Y_N Y_N^\dagger) - 72\lambda_1 \lambda_3 \text{Tr}(Y_N Y_N^\dagger) - 12\lambda_3^2 \text{Tr}(Y_N Y_N^\dagger) - 24\lambda_1 \lambda_4 \text{Tr}(Y_N Y_N^\dagger) \\
& - 6\lambda_4^2 \text{Tr}(Y_N Y_N^\dagger) - 24\lambda_5^2 \text{Tr}(Y_N Y_N^\dagger) - \frac{171}{100} g_1^4 \text{Tr}(Y_u Y_u^\dagger) - \frac{63}{10} g_1^2 g_2^2 \text{Tr}(Y_u Y_u^\dagger) \\
& - \frac{9}{4} g_2^4 \text{Tr}(Y_u Y_u^\dagger) + \frac{17}{4} g_1^2 \lambda_3 \text{Tr}(Y_u Y_u^\dagger) + \frac{45}{4} g_2^2 \lambda_3 \text{Tr}(Y_u Y_u^\dagger) + 40g_3^2 \lambda_3 \text{Tr}(Y_u Y_u^\dagger) \\
& - 72\lambda_1 \lambda_3 \text{Tr}(Y_u Y_u^\dagger) - 12\lambda_3^2 \text{Tr}(Y_u Y_u^\dagger) - 24\lambda_1 \lambda_4 \text{Tr}(Y_u Y_u^\dagger) - 6\lambda_4^2 \text{Tr}(Y_u Y_u^\dagger) \\
& - 24\lambda_5^2 \text{Tr}(Y_u Y_u^\dagger) - \frac{27}{2} \lambda_3 \text{Tr}(Y_d Y_d^\dagger Y_d Y_d^\dagger) - 21\lambda_3 \text{Tr}(Y_d Y_u^\dagger Y_u Y_d^\dagger) - 24\lambda_4 \text{Tr}(Y_d Y_u^\dagger Y_u Y_d^\dagger) \\
& - \frac{9}{2} \lambda_3 \text{Tr}(Y_e Y_e^\dagger Y_e Y_e^\dagger) + 3\lambda_3 \text{Tr}(Y_e Y_N^\dagger Y_N Y_e^\dagger) + 8\lambda_4 \text{Tr}(Y_e Y_N^\dagger Y_N Y_e^\dagger) - \frac{45}{2} \lambda_3 \text{Tr}(Y_N Y_N^\dagger Y_N Y_N^\dagger) \\
& - \frac{27}{2} \lambda_3 \text{Tr}(Y_u Y_u^\dagger Y_u Y_u^\dagger) \Big]. \\
\beta_{\lambda_4} = & \frac{1}{16\pi^2} \left[\frac{9}{5} g_1^2 g_2^2 - \frac{9}{5} g_1^2 \lambda_4 - 9g_2^2 \lambda_4 + 4\lambda_1 \lambda_4 + 4\lambda_2 \lambda_4 + 8\lambda_3 \lambda_4 + 4\lambda_4^2 + 32\lambda_5^2 + 6\lambda_4 \text{Tr}(Y_d Y_d^\dagger) \right. \\
& \left. + 2\lambda_4 \text{Tr}(Y_e Y_e^\dagger) + 6\lambda_4 \text{Tr}(Y_N Y_N^\dagger) + 6\lambda_4 \text{Tr}(Y_u Y_u^\dagger) \right] \\
& + \frac{1}{(16\pi^2)^2} \left[-\frac{657}{50} g_1^4 g_2^2 - \frac{106}{5} g_1^2 g_2^4 + 6g_1^2 g_2^2 \lambda_1 + 6g_1^2 g_2^2 \lambda_2 + \frac{6}{5} g_1^2 g_2^2 \lambda_3 + \frac{1413}{200} g_1^4 \lambda_4 + \frac{153}{20} g_1^2 g_2^2 \lambda_4 \right. \\
& + \frac{89}{8} g_2^4 \lambda_4 + \frac{24}{5} g_1^2 \lambda_1 \lambda_4 - 28\lambda_1^2 \lambda_4 + \frac{24}{5} g_1^2 \lambda_2 \lambda_4 - 28\lambda_2^2 \lambda_4 + \frac{12}{5} g_1^2 \lambda_3 \lambda_4 + 36g_2^2 \lambda_3 \lambda_4 \\
& - 80\lambda_1 \lambda_3 \lambda_4 - 80\lambda_2 \lambda_3 \lambda_4 - 28\lambda_3^2 \lambda_4 + \frac{24}{5} g_1^2 \lambda_4^2 + 18g_2^2 \lambda_4^2 - 40\lambda_1 \lambda_4^2 - 40\lambda_2 \lambda_4^2 - 28\lambda_3 \lambda_4^2 \\
& + \frac{192}{5} g_1^2 \lambda_5^2 + 216g_2^2 \lambda_5^2 - 192\lambda_1 \lambda_5^2 - 192\lambda_2 \lambda_5^2 - 192\lambda_3 \lambda_5^2 - 104\lambda_4 \lambda_5^2 \\
& + \left(4 \left(10g_3^2 \lambda_4 - 3 \left(2\lambda_1 \lambda_4 + 2\lambda_3 \lambda_4 + 8\lambda_5^2 + \lambda_4^2 \right) \right) + \frac{45}{4} g_2^2 \lambda_4 + g_1^2 \left(\frac{27}{5} g_2^2 + \frac{5}{4} \lambda_4 \right) \right) \text{Tr}(Y_d Y_d^\dagger) \\
& + \left(-4 \left(2\lambda_1 \lambda_4 + 2\lambda_3 \lambda_4 + 8\lambda_5^2 + \lambda_4^2 \right) + \frac{15}{4} g_2^2 \lambda_4 + \frac{3}{20} g_1^2 (25\lambda_4 + 44g_2^2) \right) \text{Tr}(Y_e Y_e^\dagger) \\
& - \frac{57}{5} g_1^2 g_2^2 \text{Tr}(Y_N Y_N^\dagger) + \frac{9}{4} g_1^2 \lambda_4 \text{Tr}(Y_N Y_N^\dagger) + \frac{165}{4} g_2^2 \lambda_4 \text{Tr}(Y_N Y_N^\dagger) - 24\lambda_1 \lambda_4 \text{Tr}(Y_N Y_N^\dagger) \\
& - 24\lambda_3 \lambda_4 \text{Tr}(Y_N Y_N^\dagger) - 12\lambda_4^2 \text{Tr}(Y_N Y_N^\dagger) - 96\lambda_5^2 \text{Tr}(Y_N Y_N^\dagger) + \frac{63}{5} g_1^2 g_2^2 \text{Tr}(Y_u Y_u^\dagger) \\
& + \frac{17}{4} g_1^2 \lambda_4 \text{Tr}(Y_u Y_u^\dagger) + \frac{45}{4} g_2^2 \lambda_4 \text{Tr}(Y_u Y_u^\dagger) + 40g_3^2 \lambda_4 \text{Tr}(Y_u Y_u^\dagger) - 24\lambda_1 \lambda_4 \text{Tr}(Y_u Y_u^\dagger) \\
& - 24\lambda_3 \lambda_4 \text{Tr}(Y_u Y_u^\dagger) - 12\lambda_4^2 \text{Tr}(Y_u Y_u^\dagger) - 96\lambda_5^2 \text{Tr}(Y_u Y_u^\dagger) - \frac{27}{2} \lambda_4 \text{Tr}(Y_d Y_d^\dagger Y_d Y_d^\dagger) \\
& + 27\lambda_4 \text{Tr}(Y_d Y_u^\dagger Y_u Y_d^\dagger) - \frac{9}{2} \lambda_4 \text{Tr}(Y_e Y_e^\dagger Y_e Y_e^\dagger) - 13\lambda_4 \text{Tr}(Y_e Y_N^\dagger Y_N Y_e^\dagger) - \frac{45}{2} \lambda_4 \text{Tr}(Y_N Y_N^\dagger Y_N Y_N^\dagger) \\
& \left. - \frac{27}{2} \lambda_4 \text{Tr}(Y_u Y_u^\dagger Y_u Y_u^\dagger) \right].
\end{aligned}$$

$$\begin{aligned}
\beta_{\lambda_5} = & \frac{1}{16\pi^2} \left[-\frac{9}{5}g_1^2\lambda_5 - 9g_2^2\lambda_5 + 4\lambda_1\lambda_5 + 4\lambda_2\lambda_5 + 8\lambda_3\lambda_5 + 12\lambda_4\lambda_5 + 6\lambda_5\text{Tr}(Y_d Y_d^\dagger) + 2\lambda_5\text{Tr}(Y_e Y_e^\dagger) \right. \\
& \left. + 6\lambda_5\text{Tr}(Y_N Y_N^\dagger) + 6\lambda_5\text{Tr}(Y_u Y_u^\dagger) \right] \\
& + \frac{1}{(16\pi^2)^2} \left[\frac{1413}{200}g_1^4\lambda_5 + \frac{57}{20}g_1^2g_2^2\lambda_5 + \frac{89}{8}g_2^4\lambda_5 - \frac{12}{5}g_1^2\lambda_1\lambda_5 - 28\lambda_1^2\lambda_5 - \frac{12}{5}g_1^2\lambda_2\lambda_5 - 28\lambda_2^2\lambda_5 \right. \\
& + \frac{48}{5}g_1^2\lambda_3\lambda_5 + 36g_2^2\lambda_3\lambda_5 - 80\lambda_1\lambda_3\lambda_5 - 80\lambda_2\lambda_3\lambda_5 - 28\lambda_3^2\lambda_5 + \frac{72}{5}g_1^2\lambda_4\lambda_5 + 72g_2^2\lambda_4\lambda_5 \\
& - 88\lambda_1\lambda_4\lambda_5 - 88\lambda_2\lambda_4\lambda_5 - 76\lambda_3\lambda_4\lambda_5 - 32\lambda_4^2\lambda_5 + 24\lambda_5^3 \\
& + \frac{1}{4} \left(16(10g_3^2 - 6\lambda_1 - 6\lambda_3 - 9\lambda_4) + 45g_2^2 + 5g_1^2 \right) \lambda_5 \text{Tr}(Y_d Y_d^\dagger) \\
& + \frac{1}{4} \left(15g_1^2 + 15g_2^2 - 16(2\lambda_1 + 2\lambda_3 + 3\lambda_4) \right) \lambda_5 \text{Tr}(Y_e Y_e^\dagger) + \frac{9}{4}g_1^2\lambda_5 \text{Tr}(Y_N Y_N^\dagger) + \frac{165}{4}g_2^2\lambda_5 \text{Tr}(Y_N Y_N^\dagger) \\
& - 24\lambda_1\lambda_5 \text{Tr}(Y_N Y_N^\dagger) - 24\lambda_3\lambda_5 \text{Tr}(Y_N Y_N^\dagger) - 36\lambda_4\lambda_5 \text{Tr}(Y_N Y_N^\dagger) + \frac{17}{4}g_1^2\lambda_5 \text{Tr}(Y_u Y_u^\dagger) \\
& + \frac{45}{4}g_2^2\lambda_5 \text{Tr}(Y_u Y_u^\dagger) + 40g_3^2\lambda_5 \text{Tr}(Y_u Y_u^\dagger) - 24\lambda_1\lambda_5 \text{Tr}(Y_u Y_u^\dagger) - 24\lambda_3\lambda_5 \text{Tr}(Y_u Y_u^\dagger) \\
& - 36\lambda_4\lambda_5 \text{Tr}(Y_u Y_u^\dagger) - \frac{3}{2}\lambda_5 \text{Tr}(Y_d Y_d^\dagger Y_d Y_d^\dagger) + 3\lambda_5 \text{Tr}(Y_d Y_u^\dagger Y_u Y_d^\dagger) - \frac{1}{2}\lambda_5 \text{Tr}(Y_e Y_e^\dagger Y_e Y_e^\dagger) \\
& - 21\lambda_5 \text{Tr}(Y_e Y_N^\dagger Y_N Y_e^\dagger) - \frac{5}{2}\lambda_5 \text{Tr}(Y_N Y_N^\dagger Y_N Y_N^\dagger) - \frac{3}{2}\lambda_5 \text{Tr}(Y_u Y_u^\dagger Y_u Y_u^\dagger) \left. \right].
\end{aligned}$$

A.2 Yukawa Coupling

$$\begin{aligned}
\beta_{Y_u} = & \frac{1}{16\pi^2} \left[-\frac{3}{2} \left(-Y_u Y_u^\dagger Y_u + Y_u Y_d^\dagger Y_d \right) \right. \\
& \left. + Y_u \left(3\text{Tr}(Y_d Y_d^\dagger) + 3\text{Tr}(Y_N Y_N^\dagger) + 3\text{Tr}(Y_u Y_u^\dagger) - 8g_3^2 - \frac{17}{20}g_1^2 - \frac{9}{4}g_2^2 + \text{Tr}(Y_e Y_e^\dagger) \right) \right] \\
& + \frac{1}{(16\pi^2)^2} \left[\frac{1}{80} \left(20 \left(11Y_u Y_d^\dagger Y_d Y_d^\dagger Y_d - 4Y_u Y_u^\dagger Y_u Y_d^\dagger Y_d + 6Y_u Y_u^\dagger Y_u Y_u^\dagger Y_u - Y_u Y_d^\dagger Y_d Y_u^\dagger Y_u \right) \right. \right. \\
& + Y_u Y_u^\dagger Y_u \left(1280g_3^2 - 180\text{Tr}(Y_e Y_e^\dagger) + 223g_1^2 - 540\text{Tr}(Y_d Y_d^\dagger) - 540\text{Tr}(Y_N Y_N^\dagger) - 540\text{Tr}(Y_u Y_u^\dagger) \right. \\
& + Y_u Y_d^\dagger Y_d \left(100\text{Tr}(Y_e Y_e^\dagger) - 1280g_3^2 + 300\text{Tr}(Y_d Y_d^\dagger) + 300\text{Tr}(Y_N Y_N^\dagger) + 300\text{Tr}(Y_u Y_u^\dagger) - 43g_1^2 + 45g_2^2 \right) \\
& + Y_u \left(\frac{1267}{600}g_1^4 - \frac{9}{20}g_1^2g_2^2 - \frac{5}{4}g_2^4 + \frac{19}{15}g_1^2g_3^2 + 9g_2^2g_3^2 - 108g_3^4 + 6\lambda_1^2 + \lambda_3^2 + \lambda_3\lambda_4 + \lambda_4^2 + 6\lambda_5^2 \right. \\
& + \frac{5}{8} \left(32g_3^2 + 9g_2^2 + g_1^2 \right) \text{Tr}(Y_d Y_d^\dagger) + \frac{15}{8} \left(g_1^2 + g_2^2 \right) \text{Tr}(Y_e Y_e^\dagger) + \frac{9}{8}g_1^2\text{Tr}(Y_N Y_N^\dagger) + \frac{165}{8}g_2^2\text{Tr}(Y_N Y_N^\dagger) \\
& + \frac{17}{8}g_1^2\text{Tr}(Y_u Y_u^\dagger) + \frac{45}{8}g_2^2\text{Tr}(Y_u Y_u^\dagger) + 20g_3^2\text{Tr}(Y_u Y_u^\dagger) - \frac{27}{4}\text{Tr}(Y_d Y_d^\dagger Y_d Y_d^\dagger) \\
& + \frac{3}{2}\text{Tr}(Y_d Y_u^\dagger Y_u Y_d^\dagger) - \frac{9}{4}\text{Tr}(Y_e Y_e^\dagger Y_e Y_e^\dagger) - \frac{21}{2}\text{Tr}(Y_e Y_N^\dagger Y_N Y_e^\dagger) - \frac{45}{4}\text{Tr}(Y_N Y_N^\dagger Y_N Y_N^\dagger) \\
& \left. \left. - \frac{27}{4}\text{Tr}(Y_u Y_u^\dagger Y_u Y_u^\dagger) \right) \right] + 675g_2^2 - 960\lambda_1 \left. \right].
\end{aligned}$$

References

- [1] G. Aad *et al.* [ATLAS Collaboration], Phys. Lett. B **716**, 1 (2012) [arXiv:1207.7214 [hep-ex]].
- [2] S. Chatrchyan *et al.* [CMS Collaboration], Phys. Lett. B **716**, 30 (2012) [arXiv:1207.7235 [hep-ex]].
- [3] G. Aad *et al.* [ATLAS Collaboration], Phys. Lett. B **726**, 120 (2013) [arXiv:1307.1432 [hep-ex]].
- [4] A. M. Sirunyan *et al.* [CMS Collaboration], Eur. Phys. J. C **79**, no. 5, 421 (2019) [arXiv:1809.10733 [hep-ex]].
- [5] The ATLAS collaboration [ATLAS Collaboration], ATLAS-CONF-2018-031.
- [6] G. Isidori, G. Ridolfi and A. Strumia, Nucl. Phys. B **609**, 387 (2001) [hep-ph/0104016].
- [7] F. Bezrukov, M. Y. Kalmykov, B. A. Kniehl and M. Shaposhnikov, JHEP **1210**, 140 (2012) [arXiv:1205.2893 [hep-ph]].
- [8] G. Degrandi, S. Di Vita, J. Elias-Miro, J. R. Espinosa, G. F. Giudice, G. Isidori and A. Strumia, JHEP **1208**, 098 (2012) [arXiv:1205.6497 [hep-ph]].
- [9] D. Buttazzo, G. Degrandi, P. P. Giardino, G. F. Giudice, F. Sala, A. Salvio and A. Strumia, JHEP **1312**, 089 (2013) [arXiv:1307.3536 [hep-ph]].
- [10] M. Gonderinger, H. Lim and M. J. Ramsey-Musolf, Phys. Rev. D **86** (2012) 043511 doi:10.1103/PhysRevD.86.043511 [arXiv:1202.1316 [hep-ph]]. M. Gonderinger, Y. Li, H. Patel and M. J. Ramsey-Musolf, JHEP **1001** (2010) 053 doi:10.1007/JHEP01(2010)053 [arXiv:0910.3167 [hep-ph]]. R. Costa, A. P. Morais, M. O. P. Sampaio and R. Santos, Phys. Rev. D **92** (2015) 025024 doi:10.1103/PhysRevD.92.025024 [arXiv:1411.4048 [hep-ph]]. N. Haba and Y. Yamaguchi, PTEP **2015** (2015) no.9, 093B05 doi:10.1093/ptep/ptv121 [arXiv:1504.05669 [hep-ph]]. W. L. Guo and Y. L. Wu, JHEP **1010** (2010) 083 doi:10.1007/JHEP10(2010)083 [arXiv:1006.2518 [hep-ph]]. V. Barger, P. Langacker, M. McCaskey, M. Ramsey-Musolf and G. Shaughnessy, Phys. Rev. D **79** (2009) 015018 doi:10.1103/PhysRevD.79.015018 [arXiv:0811.0393 [hep-ph]]. N. Khan and S. Rakshit, Phys. Rev. D **90** (2014) no.11, 113008 doi:10.1103/PhysRevD.90.113008 [arXiv:1407.6015 [hep-ph]]. S. Baek, P. Ko, W. I. Park and E. Senaha, JHEP **1211** (2012) 116 doi:10.1007/JHEP11(2012)116 [arXiv:1209.4163 [hep-ph]]. A. Datta, A. Elsayed, S. Khalil and A. Moursy, Phys. Rev. D **88**, no. 5, 053011 (2013) [arXiv:1308.0816 [hep-ph]]. J. Chakraborty, P. Konar and T. Mondal, Phys. Rev. D **89**, no. 5, 056014 (2014) [arXiv:1308.1291 [hep-ph]].
- [11] P. Bandyopadhyay and R. Mandal, Phys. Rev. D **95** (2017) no.3, 035007 [arXiv:1609.03561 [hep-ph]].
- [12] N. Chakraborty and B. Mukhopadhyaya, Eur. Phys. J. C **77** (2017) no.3, 153 doi:10.1140/epjc/s10052-017-4705-0 [arXiv:1603.05883 [hep-ph]]. I. Chakraborty and

- A. Kundu, Phys. Rev. D **92** (2015) no.9, 095023 doi:10.1103/PhysRevD.92.095023 [arXiv:1508.00702 [hep-ph]]. P. M. Ferreira, R. Santos and A. Barroso, Phys. Lett. B **603**, 219 (2004) Erratum: [Phys. Lett. B **629**, 114 (2005)] [hep-ph/0406231]. M. Maniatis, A. von Manteuffel, O. Nachtmann and F. Nagel, Eur. Phys. J. C **48**, 805 (2006) [hep-ph/0605184]. A. Barroso, P. M. Ferreira, R. Santos and J. P. Silva, Phys. Rev. D **74**, 085016 (2006) [hep-ph/0608282]. R. A. Battye, G. D. Brawn and A. Pilaftsis, JHEP **1108**, 020 (2011) [arXiv:1106.3482 [hep-ph]]. K. Kannike, Eur. Phys. J. C **76**, no. 6, 324 (2016) Erratum: [Eur. Phys. J. C **78**, no. 5, 355 (2018)] [arXiv:1603.02680 [hep-ph]]. X. J. Xu, Phys. Rev. D **95**, no. 11, 115019 (2017) [arXiv:1705.08965 [hep-ph]].
- [13] N. Haba and Y. Yamaguchi, PTEP **2015**, no. 9, 093B05 (2015) [arXiv:1504.05669 [hep-ph]]. S. Oda, N. Okada and D. s. Takahashi, Phys. Rev. D **92**, no. 1, 015026 (2015) [arXiv:1504.06291 [hep-ph]]. Eur. Phys. J. C **77**, no. 2, 122 (2017) [arXiv:1509.01466 [hep-ph]]. A. Das, S. Oda, N. Okada and D. s. Takahashi, Phys. Rev. D **93**, no. 11, 115038 (2016) [arXiv:1605.01157 [hep-ph]]. P. Ghosh, A. K. Saha and A. Sil, Phys. Rev. D **97**, no. 7, 075034 (2018) [arXiv:1706.04931 [hep-ph]].
- [14] N. Chakrabarty, D. K. Ghosh, B. Mukhopadhyaya and I. Saha, Phys. Rev. D **92** (2015) no.1, 015002 doi:10.1103/PhysRevD.92.015002 [arXiv:1501.03700 [hep-ph]]. B. Swiezeska, JHEP **1507** (2015) 118 doi:10.1007/JHEP07(2015)118 [arXiv:1503.07078 [hep-ph]]. N. Khan and S. Rakshit, Phys. Rev. D **92** (2015) 055006 doi:10.1103/PhysRevD.92.055006 [arXiv:1503.03085 [hep-ph]].
- [15] A. Belyaev, G. Cacciapaglia, I. P. Ivanov, F. Rojas-Abatte and M. Thomas, Phys. Rev. D **97** (2018) no.3, 035011 doi:10.1103/PhysRevD.97.035011 [arXiv:1612.00511 [hep-ph]].
- [16] S. Jangid and P. Bandyopadhyay, [arXiv:2003.11821 [hep-ph]].
- [17] S. Yaser Ayazi and S. M. Firouzabadi, Cogent Phys. **2** (2015) 1047559 doi:10.1080/23311940.2015.1047559 [arXiv:1501.06176 [hep-ph]]. N. Khan, Eur. Phys. J. C **78** (2018) no.4, 341 doi:10.1140/epjc/s10052-018-5766-4 [arXiv:1610.03178 [hep-ph]]. I. Gogoladze, N. Okada and Q. Shafi, Phys. Rev. D **78**, 085005 (2008) [arXiv:0802.3257 [hep-ph]]. E. J. Chun, H. M. Lee and P. Sharma, JHEP **1211**, 106 (2012) [arXiv:1209.1303 [hep-ph]]. P. S. B. Dev, D. K. Ghosh, N. Okada and I. Saha, JHEP **1303**, 150 (2013) Erratum: [JHEP **1305**, 049 (2013)] [arXiv:1301.3453 [hep-ph]]. A. Kobakhidze and A. Spencer-Smith, JHEP **1308**, 036 (2013) [arXiv:1305.7283 [hep-ph]]. C. Bonilla, R. M. Fonseca and J. W. F. Valle, Phys. Rev. D **92**, no. 7, 075028 (2015) [arXiv:1508.02323 [hep-ph]]. N. Haba, H. Ishida, N. Okada and Y. Yamaguchi, Eur. Phys. J. C **76**, no. 6, 333 (2016) [arXiv:1601.05217 [hep-ph]]. P. S. B. Dev, C. M. Vila and W. Rodejohann, Nucl. Phys. B **921**, 436 (2017) [arXiv:1703.00828 [hep-ph]].
- [18] R. N. Mohapatra, Phys. Rev. D **34**, 909 (1986). P. S. B. Dev, R. N. Mohapatra, W. Rodejohann and X. J. Xu, JHEP **1902**, 154 (2019) [arXiv:1811.06869 [hep-ph]]. G. Chauhan, arXiv:1907.07153 [hep-ph].

- [19] P. Bandyopadhyay, P. S. Bhupal Dev, S. Jangid and A. Kumar, [arXiv:2001.01764 [hep-ph]].
- [20] C. Coriano, L. Delle Rose and C. Marzo, Phys. Lett. B **738** (2014) 13
doi:10.1016/j.physletb.2014.09.001 [arXiv:1407.8539 [hep-ph]].
- [21] C. Coriano, L. Delle Rose and C. Marzo, JHEP **1602** (2016) 135
doi:10.1007/JHEP02(2016)135 [arXiv:1510.02379 [hep-ph]].
- [22] L. Delle Rose, C. Marzo and A. Urbano, JHEP **1512** (2015) 050
doi:10.1007/JHEP12(2015)050 [arXiv:1506.03360 [hep-ph]].
- [23] I. Garg, S. Goswami, K. N. Vishnudath and N. Khan, Phys. Rev. D **96** (2017) no.5, 055020 doi:10.1103/PhysRevD.96.055020 [arXiv:1706.08851 [hep-ph]].
- [24] J. A. Casas, V. Di Clemente, A. Ibarra and M. Quiros, Phys. Rev. D **62**, 053005 (2000) [hep-ph/9904295].
- [25] J. Elias-Miro, J. R. Espinosa, G. F. Giudice, G. Isidori, A. Riotto and A. Strumia, Phys. Lett. B **709**, 222 (2012) [arXiv:1112.3022 [hep-ph]].
- [26] W. Rodejohann and H. Zhang, JHEP **1206**, 022 (2012) [arXiv:1203.3825 [hep-ph]].
- [27] I. Masina, Phys. Rev. D **87**, no. 5, 053001 (2013) [arXiv:1209.0393 [hep-ph]].
- [28] M. Farina, D. Pappadopulo and A. Strumia, JHEP **1308**, 022 (2013) [arXiv:1303.7244 [hep-ph]].
- [29] J. N. Ng and A. de la Puente, Eur. Phys. J. C **76**, no. 3, 122 (2016) [arXiv:1510.00742 [hep-ph]].
- [30] G. Bambhaniya, P. S. B. Dev, S. Goswami, S. Khan and W. Rodejohann, Phys. Rev. D **95**, no. 9, 095016 (2017) [arXiv:1611.03827 [hep-ph]].
- [31] S. Khan, S. Goswami and S. Roy, Phys. Rev. D **89**, no. 7, 073021 (2014) [arXiv:1212.3694 [hep-ph]].
- [32] A. Das, S. Goswami, K. N. Vishnudath and T. Nomura, arXiv:1905.00201 [hep-ph].
- [33] S. Baek, P. Ko, W. I. Park and E. Senaha, JHEP **1211**, 116 (2012) [arXiv:1209.4163 [hep-ph]].
- [34] M. Lindner, M. Platscher, C. E. Yaguna and A. Merle, Phys. Rev. D **94**, no. 11, 115027 (2016) [arXiv:1608.00577 [hep-ph]].
- [35] A. Dutta Banik, A. K. Saha and A. Sil, Phys. Rev. D **98**, no. 7, 075013 (2018) [arXiv:1806.08080 [hep-ph]].
- [36] J. W. Wang, X. J. Bi, P. F. Yin and Z. H. Yu, Phys. Rev. D **99**, no. 5, 055009 (2019) [arXiv:1811.08743 [hep-ph]].
- [37] M. L. Xiao and J. H. Yu, Phys. Rev. D **90**, no. 1, 014007 (2014) Addendum: [Phys. Rev. D **90**, no. 1, 019901 (2014)] [arXiv:1404.0681 [hep-ph]].
- [38] S. Gopalakrishna and A. Velusamy, Phys. Rev. D **99**, no. 11, 115020 (2019) [arXiv:1812.11303 [hep-ph]].

- [39] R. N. Mohapatra and Y. Zhang, JHEP **1406**, 072 (2014) [arXiv:1401.6701 [hep-ph]].
- [40] P. S. B. Dev, R. N. Mohapatra and Y. Zhang, JHEP **1602**, 186 (2016) [arXiv:1512.08507 [hep-ph]].
- [41] M. Tanabashi *et al.* [Particle Data Group], Phys. Rev. D **98**, no. 3, 030001 (2018).
- [42] T. Markkanen, A. Rajantie and S. Stopyra, Front. Astron. Space Sci. **5**, 40 (2018) [arXiv:1809.06923 [astro-ph.CO]].
- [43] J. R. Espinosa, PoS TOP **2015** (2016) 043 [arXiv:1512.01222 [hep-ph]].
- [44] R. Franceschini, T. Hambye and A. Strumia, Phys. Rev. D **78** (2008), 033002 doi:10.1103/PhysRevD.78.033002 [arXiv:0805.1613 [hep-ph]]. R. Foot, H. Lew, X. G. He and G. C. Joshi, Z. Phys. C **44** (1989) 441.
- [45] P. Bandyopadhyay and E. J. Chun, JHEP **11** (2010), 006 doi:10.1007/JHEP11(2010)006 [arXiv:1007.2281 [hep-ph]].
- [46] P. Bandyopadhyay, S. Choi, E. J. Chun and K. Min, Phys. Rev. D **85** (2012), 073013 doi:10.1103/PhysRevD.85.073013 [arXiv:1112.3080 [hep-ph]].
- [47] P. Bandyopadhyay, S. Choubey and M. Mitra, JHEP **10** (2009), 012 doi:10.1088/1126-6708/2009/10/012 [arXiv:0906.5330 [hep-ph]].
- [48] R. Ruiz, JHEP **12** (2015), 165 doi:10.1007/JHEP12(2015)165 [arXiv:1509.05416 [hep-ph]].
- [49] A. Das and S. Mandal, [arXiv:2006.04123 [hep-ph]].
- [50] A. Das, S. Mandal and T. Modak, [arXiv:2005.02267 [hep-ph]].
- [51] S. Jana, N. Okada and D. Raut, [arXiv:1911.09037 [hep-ph]].
- [52] M. Mitra, S. Niyogi and M. Spannowsky, Phys. Rev. D **95** (2017) no.3, 035042 doi:10.1103/PhysRevD.95.035042 [arXiv:1611.09594 [hep-ph]].
- [53] S. K. Garg, D. Goswami and P. Poullose, J. Phys. Conf. Ser. **481** (2014), 012018 doi:10.1088/1742-6596/481/1/012018
- [54] P. Bandyopadhyay, S. Dutta and M. Jakkapu, [arXiv:2007.12997 [hep-ph]].
- [55] I. Gogoladze, N. Okada and Q. Shafi, Phys. Lett. B **668**, 121 (2008) [arXiv:0805.2129 [hep-ph]].
- [56] C. S. Chen and Y. Tang, JHEP **1204**, 019 (2012) [arXiv:1202.5717 [hep-ph]].
- [57] M. Lindner, H. H. Patel and B. RadovÄiÄč, Phys. Rev. D **93**, no. 7, 073005 (2016) [arXiv:1511.06215 [hep-ph]].
- [58] S. Goswami, K. N. Vishnudath and N. Khan, Phys. Rev. D **99**, no. 7, 075012 (2019) [arXiv:1810.11687 [hep-ph]].
- [59] S. Choubey and A. Kumar, JHEP **1711** (2017) 080 doi:10.1007/JHEP11(2017)080 [arXiv:1707.06587 [hep-ph]].

- [81] P. Bandyopadhyay, E. J. Chun and R. Mandal, JHEP **1908** (2019) 169 [arXiv:1904.09494 [hep-ph]].
- [82] S. Ipek, A. D. Plascencia and J. Turner, JHEP **1812** (2018) 111 doi:10.1007/JHEP12(2018)111 [arXiv:1806.00460 [hep-ph]].
- [83] F. Staub, Comput. Phys. Commun. **185**, 1773 (2014) [arXiv:1309.7223 [hep-ph]].
- [84] S. R. Coleman and E. J. Weinberg, Phys. Rev. D **7** (1973) 1888.
- [85] J. A. Casas, J. R. Espinosa, M. Quiros and A. Riotto, Nucl. Phys. B **436**, 3 (1995) Erratum: [Nucl. Phys. B **439**, 466 (1995)] [hep-ph/9407389].
- [86] B. Eiteneuer, A. Goudelis and J. Heisig, Eur. Phys. J. C **77** (2017) no.9, 624 doi:10.1140/epjc/s10052-017-5166-1 [arXiv:1705.01458 [hep-ph]].
- [87] M. A. D'Ãaz, B. Koch and S. Urrutia-Quiroga, Adv. High Energy Phys. **2016** (2016) 8278375 doi:10.1155/2016/8278375 [arXiv:1511.04429 [hep-ph]].
- [88] C. Garcia-Cely and A. Ibarra, Nucl. Part. Phys. Proc. **263-264** (2015) 107. doi:10.1016/j.nuclphysbps.2015.04.020 S. Bhattacharya, P. Ghosh, A. K. Saha and A. Sil, arXiv:1905.12583 [hep-ph].
- [89] J. Kopp, Phys. Rev. D **88** (2013), 076013 doi:10.1103/PhysRevD.88.076013 [arXiv:1304.1184 [hep-ph]].
- [90] P. Bandyopadhyay, A. Costantini, in preparation
- [91] P. Bandyopadhyay, K. Huitu and S. Niyogi, JHEP **07** (2016), 015 doi:10.1007/JHEP07(2016)015 [arXiv:1512.09241 [hep-ph]].
- [92] P. Bandyopadhyay, C. CorianÃs and A. Costantini, Phys. Rev. D **94** (2016) no.5, 055030 doi:10.1103/PhysRevD.94.055030 [arXiv:1512.08651 [hep-ph]].
- [93] P. Bandyopadhyay, K. Huitu and A. Sabanci Keceli, JHEP **05** (2015), 026 doi:10.1007/JHEP05(2015)026 [arXiv:1412.7359 [hep-ph]].
- [94] P. Bandyopadhyay, E. J. Chun and J. C. Park, JHEP **1106** (2011) 129 [arXiv:1105.1652 [hep-ph]].
- [95] P. Bandyopadhyay and E. J. Chun, JHEP **1505** (2015) 045 [arXiv:1412.7312 [hep-ph]].
- [96] P. Bandyopadhyay, JHEP **1709** (2017) 052 [arXiv:1511.03842 [hep-ph]].
- [97] S. Jana, N. Okada and D. Raut, Phys. Rev. D **98** (2018) no.3, 035023 doi:10.1103/PhysRevD.98.035023 [arXiv:1804.06828 [hep-ph]].
- [98] S. Jana, N. Okada and D. Raut, [arXiv:1911.09037 [hep-ph]].
- [99] P. Bandyopadhyay, S. Dutta, A. KT, C. Sen, in preparation
- [100] A. M. Sirunyan *et al.* [CMS], Phys. Rev. Lett. **119** (2017) no.22, 221802 doi:10.1103/PhysRevLett.119.221802 [arXiv:1708.07962 [hep-ex]].